



Calhoun: The NPS Institutional Archive
DSpace Repository

Theses and Dissertations

1. Thesis and Dissertation Collection, all items

1957

Investigation of heat transfer modes across a flat metallic interface

Reams, Benton Edgington; Spry, Warren Lewis

Monterey, California: Naval Postgraduate School, 1957.

<http://hdl.handle.net/10945/14330>

Downloaded from NPS Archive: Calhoun



Calhoun is the Naval Postgraduate School's public access digital repository for research materials and institutional publications created by the NPS community. Calhoun is named for Professor of Mathematics Guy K. Calhoun, NPS's first appointed -- and published -- scholarly author.

Dudley Knox Library / Naval Postgraduate School
411 Dyer Road / 1 University Circle
Monterey, California USA 93943

<http://www.nps.edu/library>

INVESTIGATION OF HEAT
TRANSFER MODES ACROSS A
FLAT METALLIC INTERFACE

BENTON EDGINGTON REAMS
AND
WARREN LEWIS SPRY



INVESTIGATION OF HEAT TRANSFER MODES
ACROSS
A FLAT METALLIC INTERFACE

* * * * *

Benton E. Reams

Warren L. Spry



INVESTIGATION OF HEAT TRANSFER MODES

ACROSS

A FLAT METALLIC INTERFACE

by

Benton Edgington Reams

Warren Lewis Spry

and

Lieutenant, United States Navy

Lieutenant, United States Navy

Submitted in partial fulfillment of
the requirements for the degree of

MASTER OF SCIENCE
IN
MECHANICAL ENGINEERING

United States Naval Postgraduate School
Monterey, California

1 9 5 7

INVESTIGATION OF HEAT TRANSFER MODES
ACROSS
A FLAT METALLIC INTERFACE

This work is accepted as fulfilling
the thesis requirements for the degree of

MASTER OF SCIENCE
IN
MECHANICAL ENGINEERING

from the
United States Naval Postgraduate School

ABSTRACT

The thermal conductance of a flat aluminum joint was investigated under high vacuum and with air at atmospheric pressure as an included medium while varying flatness, surface roughness and "apparent" contact pressure. The conductances resulting from conduction through the included medium and conduction through the metallic contacts were found to be of the same order of magnitude. Conductance resulting from radiation was found to be negligible.

SUMMARY

The objectives of this thesis were as follows:

1. Investigation of the following parameters affecting the thermal conductance at a metallic interfacial joint: A. Variation of contact pressure, B. Absence or presence of a gaseous included medium in the interface gap, C. Variation of flatness (or waviness) and surface roughness of the metallic surfaces in contact, D. Variation of mean temperature.

2. Determination of the relative amount of heat flow by each of the following mechanisms: A. Radiation, B. Conduction through the metallic contact area, C. Conduction through the gaseous included medium.

3. Determination of metallic contact area.

"Apparent" metallic contact pressure was varied from zero to 1400 pounds per square inch. During all vacuum runs, the vacuum was maintained between 5×10^{-5} and 7×10^{-7} millimeters of mercury. A limited variation of mean interface temperature was made about 225°F. Flatness of the specimens varied from 0.0002 inches down to "optically flat." Roughness varied from 9 microinches RMS to 136 microinches RMS.

The following conclusions were reached:

1. The proportion of the total heat transferred across the interface by radiation is negligible.

2. The proportion of the total heat transferred across the interface by conduction through the included gas film increases somewhat with an increase of "apparent" interface pressure, reaches a maximum, then decreases

with a further increase in pressure, and finally appears to reach a constant value. The magnitude of this variation seems to be more sensitive to roughness than to flatness.

3. Thermal contact conductance was observed to vary linearly with "apparent" interface pressure in some cases, and with a power of the pressure in others. This variation is believed to be determined by roughness, flatness, and "apparent" interface pressure.

4. A shape factor called the "effective" metallic contact ratio was computed for the specimens tested which should prove useful in predicting quantitatively the effect of various included media with these specimens.

5. The thermal contact conductance always increases with an increase of "apparent" interface pressure, other variables being held constant. The rate of increase always remains the same or increases with pressure at least to the limits observed.

6. Thermal contact conductance decreases with an increase in roughness of the contact surfaces.

7. Thermal contact conductance increases with the degree of flatness of the contact surfaces.

8. Thermal contact conductance increases with an increase of mean interface temperature.

The experimental work was performed from October 1956 through May 1957 at the United States Naval Postgraduate School, Monterey, California.

The authors are indebted to Professor C. P. Howard for his guidance during all phases of the project. Professors E. C. Crittenden and S. H. Kalmbach of the Department of Physics and Professors F. L. Coonan, J. R. Clark and A. Goldberg of the Department of Metallurgy and Chemistry are also thanked for their advice and assistance. Laboratory technicians M. K. Anderson; D. W. Belsheim, SOC, USN; R. C. Moeller, OMC, USN; K. C. Smith and A. J. White were most helpful in the authors' efforts toward assembling the necessary auxiliary equipment. The principal machine elements were designed by the authors and built in the machine shops of the Naval Postgraduate School. Grateful acknowledgment is due to Messers R. P. Kennicott, N. Walker, K. W. Mothersell, A. B. Rasmussen, H. F. Perry and A. W. Allten for their excellent machine work in manufacturing the principal components. The authors are likewise indebted to Dr. W. F. Ko^hler of the Michaelson Laboratory, United States Naval Ordnance Test Station, China Lake, California, for his advice and assistance in the problem of surface roughness determination.

SYMBOLS

A	Area. When used with no subscript indicates "apparent" interface contact area, i.e. cross-sectional area of the specimens. (ft. ²)
C	Specific heat per unit volume. (BTU/ft. ³ °F. or cal./cm ³ °C.)
$\frac{dt}{dx}$	Temperature gradient. (°F./ft.)
h	Thermal contact conductance (BTU/ft. ² hr.°F.)
k	Thermal conductivity. (BTU/ft. ² hr.°F./ft. or cal./cm. ² sec.°C./cm.)
q	Heat transferred per unit time. (BTU/hr.)
$\frac{q}{A}$	Thermal current. (BTU/hr.ft. ²)
R	"Effective"metallic contact ratio. (a dimensionless shape factor)
s	Gap distance. (ft. or cm.)
t	Temperature. (°F. or °C.)
Δt	Temperature drop across the interface gap. (°F. or °C.)
u	Mean molecular velocity of gas. (ft./hr. or cm./sec.)
λ	Mean free path of gas molecules. (ft. or cm.)

SUBSCRIPTS

a	Value of parameter for the included gaseous medium.
m	Value of parameter for metallic contact area.
T	Value of parameter for total.
v	Value of parameter for vacuum runs.

TABLE OF CONTENTS

Item	Title	Page
	Abstract	ii
	Summary	iii
	Symbols	iv
Chapter I	Introduction	1
Chapter II	Description of Equipment	8
Chapter III	Experimental Procedures	
	A. Vacuum System	19
	B. Surface Roughness	21
	C. Test Procedures	
	1. Radiation and Vacuum Runs	25
	2. Air Runs	28
Chapter IV	Sources of Error	32
Chapter V	Experimental Results	37
Chapter VI	Discussion of Results	41
Chapter VII	Conclusions and Recommendations	51
Appendix A	Apparatus Photographs and Drawings	54
Appendix B	Summary of Experimental Data	69
Appendix C	Development of Shape Factor, R, "Effective" Metallic Contact Ratio	90
Appendix D	Development of an Expression for Heat Flow Across a Gas-Filled Gap at Low Pressures	93
	Bibliography	99

TABLE OF ILLUSTRATIONS

Figure	Title	Page
I-1	Resistance Model	4
III-C-1	Sample Data Sheet	30
III-C-2	Sample Observation Plot	31
VI-1	Equipotential Configuration Near a Point of Contact During a Vacuum Run	48
A-1	Photograph, General Equipment Layout, Air Run	54
A-2	Photograph, Specimen Stack	55
A-3	Photograph, Equipment, Vacuum Run	56
A-4	Photograph, Equipment, Radiation Run	57
A-5	Photograph, Equipment, Air Run	58
A-6	Photograph, Equipment, Plumbing	59
A-7	Photograph, General Equipment Layout, Air Run	60
A-8	Schematic of Vacuum, Water, and Air Systems	61
A-9	Electrical Wiring Schematic	62
A-10	Thermocouple Measurement Circuit	63
A-11	Thermocouple Recorder Circuit	64
A-12	Test Specimen and Thermocouple Schedule	65
A-13	Terminal Connector Detail	66
A-14	Loading Pole Detail	67
A-15	Equipment Symbols	68
B-1	Plot: Thermal Contact Conductance vs. "apparent" Interface Pressure, Rectangular Coordinates, Specimens Number 4, Non-Flat	81
B-2	Plot: Thermal Contact Conductance vs. "apparent" Interface Pressure, Semi-Log Coordinates, Specimens Number 4, Non-Flat	82

Figure	Title	Page
B-3	Plot: Thermal Contact Conductance vs. "apparent" Interface Pressure, Rectangular Coordinates, Specimens Number 3	83
B-4	Plot: Thermal Contact Conductance vs. "apparent" Interface Pressure, Semi-Log Coordinates, Specimens Number 3.	84
B-5	Plot: Thermal Contact Conductance vs. "apparent" Interface Pressure, Rectangular Coordinates, Specimens Number 4, Flat	85
B-6	Plot: Thermal Contact Conductance vs. "apparent" Interface Pressure, Semi-Log Coordinates, Specimens Number 4, Flat	86
B-7	Plot: Thermal Contact Conductance vs. Mean Interface Temperature, Air Runs	87
B-8	Plot: Thermal Contact Conductance vs. Mean Interface Temperature, Vacuum Runs	87
B-9	Plot: R vs. "apparent" Interface Pressure	88
B-10	Plot: $\frac{h_a}{h_T}$ vs. "apparent" Interface Pressure	89
D-1	Interface Gap Model	94
D-2	Interface Gap Model	95

LIST OF TABLES

Table	Title	Page
B-1	Run Data	69
B-2	Data from Curves of Table B-1	75
B-3	Meyer Hardness	77
B-4	Surface Roughness	78

I. Introduction

The problem of a thermal resistance at the interface of two metallic surfaces in contact appears to have been considered only recently, the earliest significant results which could be found in the literature having been published in 1939 by Jacobs and Starr (16). The twin problem of electrical resistance due to surface contact was investigated at about the same time by Bowden and Tabor (6).

The most recent work in the field of thermal resistance due to contact joints appears to have two main incentives:

1. In the nuclear power field, and
2. In the aircraft field.

The nuclear power field has encountered difficulty with thermal contact resistance in the fabrication of fuel elements for heterogeneous nuclear reactors. Because of corrosion problems, it was found necessary to "can" the uranium fuel elements in such materials as zirconium and aluminum. The primary coolant then passes around the exterior of the "can" material.

Theoretically, the amount of power which a nuclear reactor can produce is unlimited. Actually, the power which can be produced is limited by heat transfer considerations. F. Boeschoten (5) of the Netherlands stated in a paper presented at the International Conference on the Peaceful Uses of Atomic Energy at Geneva that:

A heterogeneous nuclear reactor with a high neutron flux requires necessarily a high rate of heat extraction from the fuel elements. If an aluminum canning is used, the coefficient of heat transfer for the aluminum-uranium surfaces must be as high as possible, because it soon becomes a limiting factor for heat extraction.

Many different methods have been tried to decrease the resistance due to the contact joint. Some of these methods include:

1. Fusing the fuel element with its cladding.
2. Obtaining a closer contact between the fuel and its can by pressure. One variation of this method was the hydrostatic collapsing of the can tubing around the fuel element described by Gurinsky, et al (11) at the Geneva Conference.
3. Introducing a gas between the contact surfaces.
4. Introducing a liquid between the contact surfaces. This method is now in use, utilizing liquid sodium.
5. Introducing a solid at the interface such as foil, powders, cements, etc.
6. Casting the fuel into the can.

The advent of aircraft with speeds greater than Mach 2 has presented the problem of thermal contact resistance to the aircraft industry. At speeds such as these, the skin temperature of the aircraft becomes an important consideration since metallurgical considerations affecting the strength of the aircraft skin place a limit on the temperatures which can be allowed. In order to keep the skin temperatures below this maximum it is necessary that the heat generated at the skin be effectively conducted away and dissipated. The thermal contact between the skin and the frame of the aircraft can be very poor, however, as a result of the thermal contact resistance. To find the affects of this resistance, work has been conducted at Syracuse University by Barzelay, Tong, and Holloway (2 and 3) sponsored by the National Advisory Committee for Aeronautics.

The effects of thermal contact resistance observed will be the same, regardless of where the problem is encountered. The methods of solving the problem, however, may be quite different, depending upon the environment. For instance, while it would not present any great problem to use liquid sodium to reduce the resistance in a nuclear reactor fuel element, this method would obviously be impractical in an aircraft application.

Heat is transmitted across the interface at the surface of contact of two flat surfaces by three methods:

1. By conduction through the points of metallic contact,
2. By conduction through the air (or other included medium) film between the surfaces, and
3. By radiation.

It should be noted that convection is not listed as one of the methods of heat transfer. Obviously, the distance between the surfaces is so small that the convection current effect, if present at all, would be of negligible value.

The metallic contact area will actually be significantly less than the apparent surface as noted by Holm (15):

If, ----, practically plane bodies were placed on top of each other, the whole covered area was often called the contact surface. It is more correct to call it the apparent contact surface, ----.

Usually very small areas of it are in real contact, because even so well ground surfaces always have a certain waviness. If they were ideally hard they would touch each other only in three points. But real bodies are always deformable. Therefore, the first contact points become enlarged to small areas and simultaneously new contact points set in. The sum of all these points or spots is the contact surface. Consequently, the pressure, p , always remains finite. The hardness, H , is the upper limit of p , and every tendency to exceed this limit leads to an irreversible deformation, plastic or splintering. The pressure in contacts has been found to be surprisingly high.

Thermal contact resistance is the resistance to heat flow across the interface by the three methods listed above. Tribus (33) in a discussion of a paper by Brunot and Buckland (8) has pictured this resistance as follows:

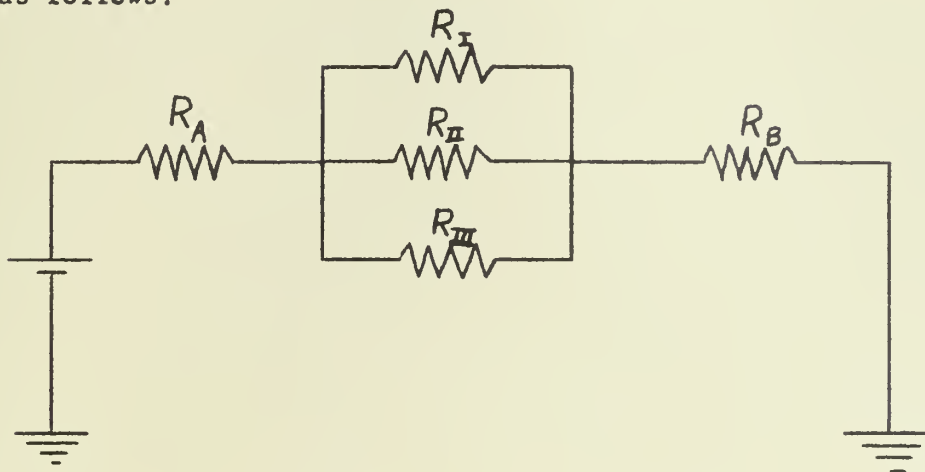


Figure I-1

Where R_I is the resistance due to conduction across the air gap, R_{II} is the resistance due to radiation across the air space, R_{III} is the resistance due to the direct metallic bond, R_A is the resistance due to conduction through the metal of the top specimen, and R_B is resistance due to conduction through the metal of the bottom specimen. Since the reciprocal of the total resistance across the joint seen by the driving potential (the temperature difference between the surfaces) is the sum of the reciprocals of the various resistances, it appears to be more convenient to use the thermal conductances rather than thermal resistances. Thermal conductance is the reciprocal of thermal resistance. Total thermal conductance across the joint is defined as the sum of the various conductances across the joint. Thermal conductance is a measure of the heat which flows between two points and since the heat

flux in the upper specimen is essentially the same as the heat flux in the lower specimen, as is pointed out in the Discussion of Results, the total heat flow (total conductance) will be the sum of the heat flow (conductance) by the various paths.

Weills and Ryder (35) have defined the thermal conductance of the gap as follows:

$$\text{Thermal conductance of gap} = h = (q/A) / \Delta t.$$

Where q/A = the thermal current, Δt = temperature drop across the gap. The thermal current can readily be calculated using Fourier's equation from McAdams (27) and measurements made during the experimental procedure as follows:

$$q = -kA \frac{dt}{dx}$$

$$\text{or } \frac{q}{A} = -k \frac{dt}{dx}$$

From this it readily follows that the thermal conductance may be defined as:

$$h = \frac{k}{\Delta t} \frac{dt}{dx}$$

This value of thermal conductance is really a fictitious or "apparent" conductance as it is made up of the various conductances described above.

Thermal contact resistance (and hence its reciprocal, the conductance) will vary with many different factors. Brunot and Buckland (8) found that:

Total resistance for unit area, i.e. "(apparent) contact area" - - will vary with smoothness, contact pressure, thermal conductivity of the metal, thermal conductivity of the gas between the metal surfaces.

Weills and Ryder (35) found that the thermal contact resistance also varied with the mean interface temperature, with the condition of the joint, and with the hardness of the metal forming the joint. These investigations have indicated that the flatness of the surface is also a parameter as noted in the Discussion of Results. As a result of time limitations the primary variables investigated by the authors were contact pressure and included medium (vacuum and air). A limited investigation of variation of thermal contact conductance with mean interface temperature was made over a small range to permit correcting the observed values of thermal conductance to a common temperature for all runs. Also a limited variation of surface roughness and flatness was investigated.

Several of the investigators in this field have speculated on the proportion of heat which flows by each of the three methods of heat transfer described above, but no quantitative results have been reported in the literature. If the mechanism of heat transfer can be evaluated, a step will have been made toward understanding thermal contact resistance and perhaps enabling quantitative predictions on the effects of included media and surface roughness. It also appeared that, in separating the various methods of heat transfer, there might be a possibility of estimating the area of metallic contact at the interface. Kouwenhoven and Potter (24) stated:

There is need for more accurate knowledge of the actual areas in contact as this remains one of the greatest unknown factors in the problem.

The idea of conducting tests in a high vacuum in order to determine the heat flow by the various methods was proposed by Keller (21) in a discussion of a paper by Weills and Ryder (35):

It would have been of great interest if at least some of the authors' tests could have been repeated with the contacts in a vacuum, and again, with the gap between the surfaces filled with a gas of much higher thermal conductivity than air, ---. By these expedients, after due allowance had been made for radiation, the relative magnitude of each of the two conductances could have been determined definitely.

Much work has been done to determine electrical contact resistance, a problem which is analogous to thermal contact resistance. There are some major differences between the two problems, however. Whereas the thermal current passes partially through the included medium, the included medium acts as an insulator in many cases for electrical current. Also tarnish films will, in general, present a greater resistance to the flow of electrical current than to the flow of thermal current. Holm (15), one of the principal investigators of this problem in the electrical field, has indicated that perhaps thermal experiments could provide information which would help clarify the problem of electrical contact resistance determination:

It should be pointed out that thin tarnish films, which may produce large electrical resistances, do not appreciably influence the thermal current. Therefore, the measurement of the thermal resistance constitutes a method for determining the load-bearing contact surface -- which is independent of any tarnish films present.



II. Description of Equipment

1. General Description.

The Equipment can be divided into the following groups:

- a. A pair of instrumented test specimens providing an interface between a common metallic material medium.
- b. A heat source for heat input and a massive heating head serving as a high temperature heat reservoir.
- c. A massive cooling head serving as a low temperature heat sink and the coolant to maintain the cooling head at low temperature.
- d. A static load device with load cell and instrumentation to determine the load.
- e. A vacuum system enclosing the test specimens and heating head.
- f. Thermal insulating material.
- g. Temperature sensing, indicating and recording devices and associated control switchboard.
- h. Power sources, safety circuits, regulator and control switchboard.
- i. Surface roughness equipment described in Chapter III B.

2. Detailed descriptions.

a. TEST SPECIMENS. Several pair of 6061, formerly designated 61-S-0, aluminum alloy test specimens were machined from a single bar. A drawing of the test specimens with the thermocouple schedule is shown in figure A-12 and the

test specimens (4)¹ show clearly in figure A-2. Conventional machining methods were used in the initial preparation of the specimens. An average flatness of the test surfaces was specified as 0.0002 inches and the two ends of each specimen were specified parallel within 0.0002 inches. These tolerances were achieved using a dial indicator and comparison with a standard surface plate. Initially, the test faces of three of the pairs of specimens were hand lapped with a third dummy block using Clover Brand Grinding and Lapping Compound grades 1A and 3A until interference fringes were clearly seen using a sodium vapor light and a DoAll A optical flat. This was undertaken to insure flatness of the specimens of the order of 100 microinches. The specimens were scribed and drilled for thermocouples to a uniform depth of 1.25 inches. Accuracy of the hole location along the vertical axis of the specimen was 0.01 inch. A hole diameter of 0.070 inches (#50 drill) was used. This resulted in a higher than desirable location tolerance, but it was considered that the "walking" tendency of a smaller drill would introduce errors which would probably do away with any accuracy gained by the use of a smaller hole. Also in order for the thermocouple to be bonded properly for vacuum work, the large hole was highly desirable.

b. HEAT SOURCE AND HEATING HEAD. Two CHROMOLOX cartridge

¹ NOTE: In this chapter a letter or number symbol enclosed in a circle indicates that the named item immediately preceding is labeled with this symbol in the figures of Appendix A. An alphabetical-numerical list of symbols is also given in the first folded page following the photographs, Figure A-15.

element heaters, model number C-503C, manufactured by the E. L. Weigan Company and rated at 250 watts each were the heat source. Their electrical input was manually controlled from a regulated supply by means of a Superior Electric Company type 116 POWERSTAT with voltage and current being determined by a Weston Electric Instrument Corporation Model 433 Voltmeter (H) and a Westinghouse Electric and Manufacturing Company style 70138 AC ammeter (G). The heating head assembly (I) is shown in figure A-2. It consists of a heavy stepped cylinder machined from a four inch bar of soft solid copper. It was drilled and tapped at each end to allow lifting of the upper test specimen to open the interface gap and thus determine the radiative transfer of heat across the gap in a high vacuum. The heater elements were inserted horizontally in the heating head and secured there by small stainless steel retaining strips.

c. COOLING HEAD. The copper cooling head (Q) was machined from the same bar as the heating head. An aluminum retaining ring was added to prevent the cooling head from being pulled upward into the vacuum jar since its maximum diameter was only slightly greater than required for the O ring seal. A pipe threaded hole was placed in one side for water entry (P) while 32 smaller radial holes extend outward from the vertical central cavity, thus permitting exit of the cooling water and insuring its contact with a relatively large surface area of the cooling head. A light galvanized steel cylinder surrounded the cooling head to catch the coolant and lead it to a drain connection (O). The cooling head proper rested on a three inch OD steel pipe which transmitted the

load to the static load machine. Two O rings sealed the entry of the cooling head through the bottom plate into the vacuum system. Cold water from the normal supply main (F) for the building was used as the coolant. An excess of coolant was employed in an attempt to insure that fluctuations in the normal supply would not unduly affect experimental results. For work requiring a constant temperature heat sink it would be necessary to provide additional auxiliary equipment as the water temperature exhibits a diurnal variation. Additional leads from the water line were utilized for the normal and shutdown cooling of the diffusion pump.

d. STATIC LOAD MACHINE. A dead weight loading machine (13) was designed for this project and constructed in the Naval Postgraduate School machine shops. It consists essentially of a V shaped base of three inch steel channel, a vertical 8 X 6-1/2 inch wide flange I-beam with fittings to receive the loading arm on the upper end, a square coaming of three inch angle iron, supported by two legs and a pair of gusset plates, to accept the bottom plate (B) and a seven foot long five inch I-beam loading arm (6) with built up positioning pads at the ends and center. Moment arms giving load ratios from 7 to 1 to a maximum of 20 to 1 are thus available and the loading machine can be used for other purposes than this experiment. The loading machine was designed to permit a maximum loading of 10,000 pounds in the 20 to 1 moment arm position. The limiting factor from the strength standpoint is the pivot pin which connects the loading arm to the pivot plate (K). The machine was designed so that this maximum load could be exerted between the loading arm and the base V as was used in this experiment or between the loading arm and the plate resting in the coaming. The maximum load of 10,000

pounds is also a safe limit in regard to stability against tipping. Should larger loads be applied, using a stronger pivot pin, it would be necessary to place weights on the rear extension of the base.

The two flat pivot plates form a movable link between the loading arm and the vertical I beam member of the machine to insure that non-axial thrust is not exerted on the loaded column of test specimens. The load was applied to the top of the heating head by a loading pole (5) of 3-1/2 inch diameter steel. The top of the pole has a 1/4 inch radius and was case hardened. It bore against a polished flat loading plate (V) of one inch thick tool steel positioned by nuts on 5/8 inch bolts extending down from the loading arm. This pole passed through the top plate (T) of the vacuum system through a double O ring seal similar to that of the cooling head. Weights were suspended from the end of the loading beam on a hanger (D) which was supported by a rod to insure vertical load application. An A frame (E) made of two inch pipe was used to support a one ton chain hoist for handling the heavy loading arm and the top plate. A lifting bracket (W) and a screw jack (X) were used to assist in separation of the interface gap for radiation readings.

Within the vacuum system, the loading pole was cut to accept a two inch section of 1/16 inch wall aluminum tubing with a 2-1/2 inch OD. Initially this load cell (J) was instrumented with two Baldwin AX-5 strain gauges in a bridge arrangement to provide temperature compensation and eliminate indication of non-axial loads. Later a strain gauge bridge was constructed using four Baldwin SR-4 A-7 bakelite bonded strain gauges to allow better performance at the high temperatures encountered (29).

The loading pole detail is shown in figure A-14. A Baldwin type M strain indicator (15) was used to determine the load on the load cell. The loading pole was placed in a recently calibrated RHIELE testing machine for purposes of calibrating the load cell before, during, and after the test program. In addition, the assembly was placed in an electric oven and the zero reading observed at various temperatures to insure that there was no variation of indicated load with temperature.

e. VACUUM SYSTEM. As previously stated, the entry of the test columns was sealed at the top and bottom plates by a pair of "O" rings. Both plates were milled from a one inch mild steel plate to 3/4 inch thickness to insure flatness, then faced on a lathe since leakage of air into the vacuum system occurred with the striations of the milling cuts. The bottom plate rested in place in the coaming of the static load machine. On the upper surface of this plate rested the 18 inch diameter vacuum tight cylinder (C) made of 1/4 inch steel. A glass cylinder was used and proved more satisfactory except for its fragility. The top plate rested on the upper end of this cylinder and both closures were sealed by a moulded neoprene gasket on the cylinder. On the bottom of the bottom plate, under a three inch hole was bolted the top flange of a water cooled oil diffusion pump (1), formerly a unit of a Navy MK 5 Optical Coating Unit. A W. M. Welch Manufacturing Company DUO-SEAL vacuum pump (2) maintained about 35 microns of pressure on the discharge arm of the diffusion pump and was connected to the latter by a flexible pipe, a series of standard pipe fittings, and a specially machined adapter. A second lead-off via a natural rubber hose was made to the vacuum cutout

switch described under h. below. Also connected here was a mercury filled Kontes Glass Company McLeod gauge (S) for measuring the fore-pressure. This measurement had no significance other than serving as a guide to the proper operation of the diffusion pump heater. (34)

The heater, located in the bottom of the diffusion pump, was controlled through a second Superior Electric type 116 POWERSTAT with current being indicated on a second Westinghouse style 70138 AC Ammeter (U). Coolant for the diffusion pump was water from the building supply system. An air connection (N) was provided for removing the water from the shutdown cooling coils of the pump prior to normal operation. An additional flexible lead from this air connection was used for leak testing the terminal connectors. All flanged joints in the vacuum system were fitted with a gasket of 1/32 inch neoprene while threaded joints were made up with Glyptal enamel. Two CENCO (Central Scientific Company) CVM glass-to-metal vacuum coupling connectors were brazed into holes in the bottom plate. A consolidated Vacuum Corporation Pirani gauge tube (M), partially visible in figure A-5, was placed in one connector and used with a Wheatstone bridge and sensitive galvanometer (12) for leak detection. The second connector on the opposite side of the loading machine held a VG-1A type ionization gauge tube (L) which means was chosen for determining the pressure in the vacuum jar. A control circuit (3) was built from plans supplied by the Department of Physics.

f. THERMAL INSULATION. In order to reduce heat loss while working in air, a heat insulating jacket (R) to surround the test column was cut from a standard 2-1/2 inch ID moulded magnesite pipe insulating shell.

The shell was scraped out so as to fit snugly around the heating head and test specimens and fitted with holes at one of the joints to permit exit of the heater and thermocouple leads. Two spacer discs and a lifting bolt of fired LAVA grade A were used as a thermal insulator between the top of the heating head and the bottom of the loading pole. Insulation here was necessary for three reasons: 1. to reduce heat losses from the system so a reasonably high mean temperature could be maintained at the interface gap; 2. to reduce the operating temperature of the load cell to an acceptable level; and 3. to assist in maintaining a constant temperature in the top plate by reducing the temperature of the loading pole. This LAVA material is naturally occurring hydrous aluminum silicate as furnished by the American Lava Corporation of Chattanooga, Tennessee. It was first machined in the ordinary manner, slightly undersized, then fired in a metallurgical furnace by raising the temperature slowly to 1800°F, holding that temperature for about 1 hour, then furnace cooled. It is credited by the supplier with 2500 pounds per square inch ultimate tensile strength, 40,000 pounds per square inch compressive strength, and a thermal conductivity $k = 0.003$ gram calorie centimeter per square centimeter second degree Centigrade. A lifting bolt made of this same material provided the means by which the heating head was attached to the loading pole during radiation readings.

g. TEMPERATURE MEASUREMENT. Eleven thermocouples were inserted in each test specimen starting 1/4 inch from the interfacial surface and spaced axially 1/4 inch apart with each successive level being displaced 100° angularly. This arrangement proved quite satisfactory since sufficient

points were available to establish a slope for determination of the interface temperature by extrapolation and by having the thermocouples angularly spaced it is believed that any appreciable disturbance of the heat flow pattern in the specimen was avoided. The Brown & Sharpe gauge 30 copper-constantan thermocouple wire was chosen because of its small size and availability. It is considered the smallest wire for practical macroscopic work in this temperature range. The fiberglass insulation and oxide coatings were removed from the wire ends with rough aluminum oxide abrasive paper. The wires at one end were twisted together then flash welded in one arm of a mercury filled U tube. This operation was difficult to perform satisfactorily unless the wires had been freshly abraded to remove the oxide film. The surface of the mercury was covered with about $\frac{1}{4}$ inch of light machine oil to quench the arc. Approximately 25 volts AC was found to give the best results. The leads were then untwisted so that the only contact occurred in the bead at the end. This end of the thermocouple was dipped in General Electric Glyptal Enamel (1201 Red) to provide physical protection and electrical insulation. After several trials with various cements, INSA-LUTE HI-TEMP CEMENT #P-7 made by Sauerseisen Cements Company was selected as the best to hold the thermocouples in the hole and to insure good thermal contact of the couple with the specimen during this high vacuum work. Brass terminal connectors, as illustrated in figure A-13 were used to transmit the thermo-electric potential through the top and bottom plates to the vacuum system. A resistance to ground of twelve megohms was required of each connector. Brown & Sharpe #24 thermocouple wire was used to carry the signal to the terminal board on the thermocouple control switchboard (8) which is illustrated in figure A-5. Each

test specimen was referenced against a separate ice junction and selector switches were connected to permit reading the absolute potential of each thermocouple and the differential voltage of any two thermocouples located in opposite specimens. The wiring diagram for this function is shown in figure A-10. An additional circuit was provided to permit selection of six thermocouples in each specimen of which three at one time could be connected to a potential recorder. A partial wiring diagram for this function is shown in figure A-11. The Leeds & Northrup Company SPEEDOMAX two point potential recorder (11) restricted observation at any one time to only one thermocouple in each specimen. This however proved sufficient to indicate the existence of a steady state temperature condition in the test specimens. For precise reading of absolute and differential values, a Rubicon precision potentiometer (10) and galvanometer (9) were used. The ice junctions were in separate kerosene filled glass tubes in a standard vacuum bottle (A) filled with crushed ice.

h. POWER SOURCES. With the exception of the SPEEDOMAX potential recorder, all AC operated equipment was furnished power through the power control switchboard (7) shown in figure A-3. The wiring diagram is given in figure A-9. Several safety circuits were necessary to permit continuous untended operation of the equipment. The diffusion pump heater was protected by a pressure switch which required a vacuum of 20-25 inches of mercury before operation was permitted, a manually reset relay which opened the circuit should the voltage supply of the fore pump motor fail, and lastly a relay connected to a Mercoid Switch (14) built by the Mercoid Corporation of Chicago, Illinois, which opened the diffusion pump heater circuit and thus the holding coil of the manually reset relay

above should the cooling water pressure fail. In addition the regulated power source for the heat source heaters was connected through the cooling water relay. The voltage regulator (16) was a Sorensen & Company model 1000 rated at one KVA and was found necessary to maintain constant voltage on the heat source because of the wide variations in the commercial supply voltage to the building. All pump and heater circuits were fused in both sides of the line at the power control switchboard and individual fuses were provided in all indicating equipment, the voltage regulator, and the POWERSTATS.

III. Experimental Procedures.

A. Vacuum System

Because of anticipated troubles in obtaining a satisfactory vacuum, this system was put into operation first. The system was built up by steps in order to facilitate trouble shooting. The fore pump was operated connected to the McLeod Gauge only. The piping system to the diffusion pump was added, and then the diffusion pump made up with a blank flange. Subsequently, the system as a whole, but without the connectors through the top and bottom plates, was operated. Finally the complete system as shown in figure A-3 was placed in operation. It was found necessary to operate the fore pump at least twenty hours before turning on the diffusion pump if unattended. However, if attended the diffusion pump could be turned on when the fore pump had reduced the pressure to less than one hundred microns. This raised the fore pressure as the diffusion pump started working. After the diffusion pump had been on for a period of about one to two hours, if the vacuum in the system could not be observed with the ionization gauge, the diffusion pump was turned off and allowed to cool. When the fore pump had restored the vacuum to less than one hundred microns the diffusion pump was again turned on and the procedure repeated. It was found that unless the system had been shut down for some time that two start-ups were sufficient to obtain proper operation of the diffusion pump. After about twenty-four hours of operation of the diffusion pump, vacuums of the order of 10^{-5} mm of Hg were obtained. The ionization gauge control circuit was checked against a commercially calibrated control circuit supplied by the Department of Physics.

Figure A-8 is a schematic of the vacuum system showing the associated water and air systems. Water cooling was provided for the section surrounding

the diffusion pump heater to prevent decomposition of the diffusion pump oil during a rapid shutdown. The air connection was provided to ensure that all water was removed from this set of coils prior to the use of the pump.

The diffusion pump requires very careful handling for trouble-free operation. If the diffusion pump heater is turned on with too high a pressure in the system the diffusion oil will decompose.

If the system is under high vacuum with the diffusion pump in operation and air is admitted suddenly, the octoil will decompose, forming long white crystals on the walls of the diffusion pump casing. Such an accident necessitates an overhauling of the pump. Should the oil, while exposed to the air, be heated accidentally, or should the vacuum be broken while the oil is still hot, the degree of decomposition will depend on the heat of the oil and the length of exposure. Provided neither the heat nor the time was too great, the oil may purify itself on subsequent operation. (34)

If the diffusion pump walls are not cooled sufficiently during operation of the heater, the vacuum system will become contaminated with oil vapor.

Since the system was operated continuously for many days when conducting vacuum runs it was necessary to provide safety circuits to prevent or minimize the troubles described above. These safety circuits are shown in figure A-9. Safety circuits were installed to provide the following:

2. 1. Shutting off the power to the diffusion pump heater if the power to the fore pump failed. Failure of the fore pump would require the diffusion pump to operate against a relatively large back pressure and would cause a loss of vacuum with its resultant deleterious effects on the oil.
2. Shutting off the power to the diffusion pump heater if the system vacuum drops below a predetermined value. This will minimize the

deterioration of the oil in case of a large air leak into the system such as would be caused by a connector, gasket or hose failure.

3. A relay to prevent the diffusion pump from restarting after a main power failure. A main power failure will cause a gradual loss of vacuum and since the length of time that the system has been shut down may be a matter of several hours it would not be desirable for the diffusion pump to restart immediately when power is restored. This relay is also tripped if any one of the other safety circuits open the diffusion pump heater circuit and must be manually reset to prevent premature re-energizing of the circuit after securing for any reason.
4. Shutting off the power to the diffusion pump and the heat source if the cooling water fails.

A pair of matched Pirani Tubes were installed, one in the vacuum system and the other, closed at the end, located adjacent to the other for temperature compensation. These tubes were connected to a bridge circuit with a sensitive galvanometer for leak detection. The bridge circuit used was a modification of a circuit recommended by Jnanananda (17). The leaks encountered were at pressures above the sensitive range of the Pirani Tubes; consequently, this system was not used to any great extent.

B. Surface Roughness

In the field of surface roughness specification there is still basic disagreement as to the use of average or RMS values and the manner of arriving at those values. An attempt has been made by American Standards

Association to define a uniform system whereby surface roughness may be specified by the designer and produced by the machinist. ASA American Standard B46.1 and Military Standard MIL-STD-10 of 2 August 1949 both cover surface roughness, waviness and lay. Also for several years, General Electric Corporation has used a set of samples as a bridge between the drawing board and the finished product. According to Mikelson (28), who described the above system, surface roughness is involved when peaks occur closer than $1/32$ inch while waviness is involved when the peaks are spaced greater than $1/32$ inch. These samples are made of steel in the form of a six inch pocket rule and for most roughnesses more than one type of cut is given. The design engineers, machinists and inspectors thus have available a prepared sample of the approximate finish desired in the completed product. Thielsch (32) advances the following warning:

Only when surfaces which have experienced similar finishing operations are compared, is examination by sight useful for even the roughest production control.

Several investigators in this field have advocated the use of optical methods of surface roughness determination in order to insure that consistent measurements were being used by all concerned. It must be recognized from the above that:

In contrast to measurements of distances, accurately and to known standards, measurements of finishes is in its infancy.
(13)

A protracted but unsuccessful attempt was made to utilize a multiple beam interferometer for precise optical measurements of the surface roughness. Briefly the procedure is expressed as follows by Sugg (31):

The optical flat with a partially reflecting film on the work side is placed on the surface of the piece to be examined, and

a series of interference fringes (light and dark bands) which follows the contour of the surface, may be observed when viewed in monochromatic light. These fringes result from interference between light beams reflected from the two surfaces in normal contact and occur at wedge thicknesses t given by the following formula $nL = 2\mu t \cos\phi$, where n is the order of interference, L the wave length of the monochromatic light, μ the refractive index of the material of the wedge, and ϕ the angle of incidence of the light. This expression reduces to $t = nL/2$ for normally incident light with air as the wedge material. The spacing between the fringes, no matter what it may be, reveals a constant half-wave-length difference in wedge thickness, and a method of measurement sensitive to a few millionths of an inch is offered. . . . Multiple band inteferometry permits the width of the dark band to be reduced to relative hairline proportions, which does reveal fine detail. . . . control the distance between fringes through control of the angle between the flat and the examined surface.

An attempt was made for higher resolving power using a metalloscope as suggested by Benford (4):

The basic design concept can of course be extended to become a higher power system by locating the microscope objective below the partially reflecting mirror, so that one can employ a traditional metallurgical microscope and vertical illuminator setup as the basis for constructing a microinterferometer. This would extend the power range, but lose the excellent design feature of a portable instrument which one can place directly on the test surface.

For this investigation only a fringe pattern was necessary; however, the warning of Loewen (25) is of interest:

Unfortunately, multiple beam interferometry has some drawbacks. The most important is that the wedge required between the mirror and work surface makes it impossible to focus the viewing microscope on both fringes and work surface simultaneously. In photographs this might be remedied by double exposure if refocusing is possible without joggling the apparatus.

This desired fringe pattern was finally obtained, but upon consulting with Dr. W. F. Ko^heler of the Michaelson Laboratory at the United States Naval Ordnance Test Station, China Lake, California, it was learned that in using this system too many variables are encountered for even

the slightest precision with the equipment available. The principal factors are the multiplicity of the reflection, the wedge angle, and the reflectivity of the optical surface. In addition, some of the roughnesses proposed for use were one order of magnitude removed from the wave length of visible light thus precluding application of this method with the means available.

A replica technique was seriously considered but this also was limited in accuracy by too many variables. This method consists of a comparison of plastic replicas of specimens of known roughness with like replicas of the specimens whose roughness measurement is desired. No calibrated specimens were available in the range desired.

Roughness measurements were taken with a Brush Surface Analyzer Model BL-103, manufactured by Brush Electronics Company with the standard PA-2 pickup head. Although the diamond stylus of a Brush Surface Analyzer probably responds principally to the crystalline hardness of the material and definitely cuts a groove in the metal being tested, this method was used as the best means available for measurement of roughness. A glass calibration standard was used to calibrate the instrument each time measurements were taken. On the roughest specimens, the roughness grooves were formed by a single spiral and all measurements with the stylus were made on a radial line. Utilization was made of the Brush Model BL-106 Averaging Meter only as an approximate check. It is not inherently accurate enough for precision work of this type. The actual roughness calculations were based on readings from the Brush oscillograph tape. The trace produced by the stylus for each of four or five positions on the specimen was "read" at 24 or more approximately regular intervals.

The resulting values were then entered into a program the authors devised for the high speed digital computer and converted to average and RMS values. The arithmetic averages of the five sets of readings were taken for the roughness values of the specimen. Measurements were made on all specimens during the authors visit to the Naval Ordnance Test Station before the specimens were initially loaded in the test apparatus. Measurements were then made with the Brush machine owned by the Postgraduate School before and after the series of runs.

From Brunot and Buckland (9) it was learned of two other ways of evaluating surfaces: (a) Average peak-to-valley distance which gives the same value for various surfaces and (b) maximum peak-to-valley distance which would give different values. According to Hagen and Lindberg (12):

The arithmetic average is $1/4$ to $1/5$ of the total peak-to-valley height for machined surfaces. For the finer finishes however, this ratio may be as small as $1/10$. For most machined surfaces it is about 10 percent less than the RMS value.

For this work it is considered that the average roughness with the maximum peak-to-valley distance specified is more significant because it is believed to be a better index of the mean free path available to the gas molecules.

C. Test Procedures.

1. Radiation and Vacuum Runs

Normally the first runs made with a set of specimens were the vacuum and radiation runs. Prior to assembling the system, the contact surfaces of the cooling and heating heads were brightened with emery paper to remove the oxide coating and then cleaned with acetone to remove all

traces of grease and other foreign material. The contact surfaces of the specimens were also cleaned with acetone. The top surface of the cooling head and the bottom surface of the heating head were coated with vacuum grease to prevent the formation of an oxide film and to assure good thermal contact with the specimens. Vacuum grease was chosen because of its low vapor pressure. The bottom specimen was put in place on the cooling head and its thermocouples made up to the connectors in the bottom plate. It was necessary to do this before placement of the vacuum jar due to the inaccessibility of the connectors with the jar in place. With the jar in place, the upper plate was suspended above the system, the top specimen was placed on the bottom one and held in vertical alignment by the Teflon guide ring, and the thermocouples from the top specimen attached to the connectors in the top plate. The heating head was put in place on the stack, secured to the top specimen by a stud, the heaters inserted, and the leads made up to connectors in the top plate. The load cell was secured to the heating head (with two Lavite discs between) with a Lavite bolt, and the strain gauge leads made up to connectors in the top plate. With the top plate suspended and held directly over the system, the loading pole was lowered through the top plate and secured to the load cell with cap screws. The top plate was lowered on to the jar and the loading arm placed in the center pivot position. Using the lifting bracket, the loading pole and thus the load cell, heating head, and top specimen were lifted sufficiently to provide a small gap at the interface between the specimens, and the vacuum pumps were started.

The system was then set up for a radiation run, and was as shown in

figure A-4. During the initial running of the vacuum system the heaters were turned on at a low power level to increase the rate of degassing and thus reduce the time required for attaining a satisfactory vacuum. A higher heater power level would have been desirable from the degassing viewpoint; however, temperature limitations required the low power level. When a satisfactory vacuum had been obtained and the stack had reached a steady state condition, the radiation runs were conducted. Since the thermal conductivity of the air in the system had been reduced to a negligible value, as shown in Appendix D, and the specimens were not in contact, any heat flow through the stack must be due to radiation. Actually other minor effects were present as discussed in the Experimental Results section.

Upon completion of the radiation runs, the loading pole was lowered, allowing the specimens to come into contact with each other and the loading arm shifted to the end pivot position. Weights were added to give a load greater than the maximum to be used during the runs to insure that all of the plastic deformation had taken place at the interface of the specimens. The weights were then removed, the loading arm shifted to the center position, and vacuum runs commenced. Weights were added in increments to the maximum allowable in this position. The system as set up for vacuum runs was as shown in figure A-3. The loading arm was then shifted to the end position and weights added to the maximum desired in this position. Readings were made at the various loads both loading and unloading. Since there was a significant friction force between the loading pole and the adjustable load carrying plate on the loading arm it was necessary to check the alignment of the system after each load change. A plumb bob was mounted

on the pivot plates and this was lined up with a vertical line parallel to the line of centers of the bearing holes for the supporting pins. Also the loading arm and the adjustable load carrying plate on the loading arm were checked horizontal after each change of load.

A sample of the data recorded is shown in Figure III-C-1. A plot was made of temperature vs. axial distance along the specimen, as shown in Figure III-C-2. From this plot mean interface temperature, temperature difference across the interface and temperature gradient were computed. From these data the thermal contact conductance was computed using the equation defined in the Introduction. A value of thermal conductivity for the aluminum of $0.43 \text{ cal./cm}^2 \text{ }^{\circ}\text{C/cm}$ was used. This value was obtained from the Aluminum Company of America (1).

C. Test Procedures

2. Air Runs

To shift to air runs from the vacuum runs, the vacuum system was shut down by first securing the diffusion pump heater and allowing the oil to cool. Then the fore pump was secured and air slowly admitted to the system by breaking the hose connection to the McLeod Gauge. The top plate was suspended above the system and the loading pole disconnected from the load cell. The load cell and the heating head were removed and the top specimen suspended from the top plate to prevent putting a strain on the thermocouple wires. The vacuum jar was removed and a wooden frame put in its place. The top plate was placed on the wooden frame and the stack reassembled. Since it was not necessary to lift the top specimen during the air runs, the stud and the Lavite bolt used in the vacuum runs were not used during air runs. The "O" Rings were removed from the top

plate during one of the air runs in order to get an estimate of their friction effect on the load. Nothing could be determined with the equipment available. Insulation was placed around the stack to reduce radiation and convection-conduction via the air surrounding the system. The load procedure was the same as that followed for the air runs with the exception that it was not necessary to pre-load the specimens as this had been previously accomplished. The same data was taken as for radiation and vacuum runs. Plots and computations made were also the same.

SAMPLE DATA SHEET

Run No. 180

Date 4-23-57 Time 1530

Specimen No. 1

Included medium air

Vacuum -- mm Hg Diffusion Pump Current -- amp.

Heaters in use #1 ☒ #2 ☒ 3.4 amp. 91.3 volts

Mean joint temperature 199.1 °F.

Weights No Load lb. Pivot position -- # of top wt --

Strain gauge reading 11870 /in./in. Load 42 lb.

Joint pressure 6 psi

Thermocouple No.	Individual		Differential	
	Upper	Lower		
	mv	Temp	mv	Temp

1	41135	205.8	open		
2	42095	209.6	36615	188.0	
3	43010	213.2	35895	185.1	
4	43930	216.7	34885	181.1	
5	44895	220.3	33975	177.5	
6	45915	224.2	32915	173.3	
7	46850	227.7	32220	170.5	
8	47760	231.1	31200	166.5	
9	48890	235.4	30200	162.5	
10	49685	238.3	shorted		
11	50710	242.1	28370	155.0	

12 (strain gauge) 28095 OK Changed Load Shift Specimens /in./in.

Figure III-C-1

RUN
180

SAMPLE OBSERVATION PLOT

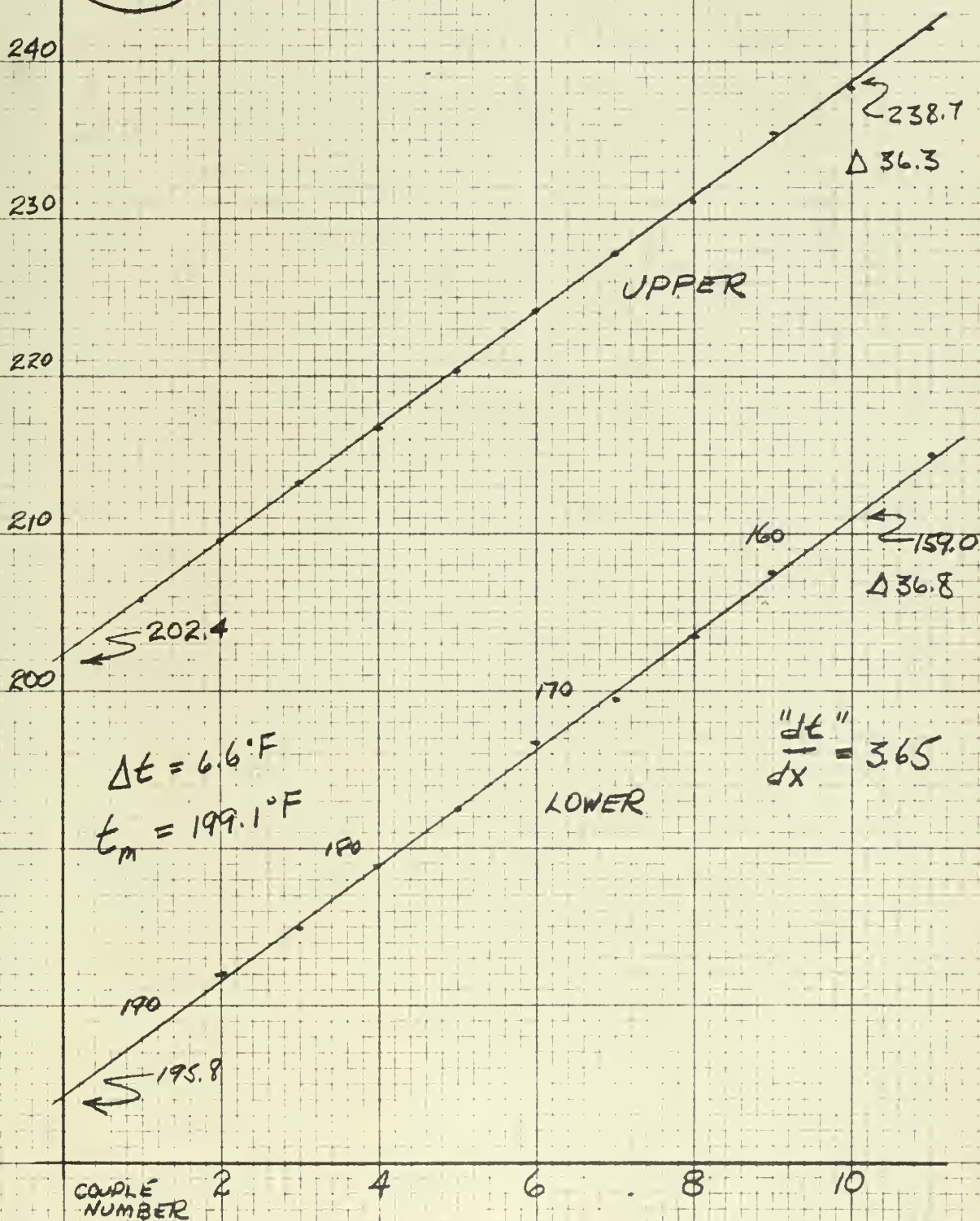


Figure III-C-2

IV. Sources of Error

To obtain an absolute value of conductance in a series of experiments of this type, with a specimen having specified characteristics, it was not considered feasible to apply the single sample analysis technique (23) to each of the possible deviations of the many variables. For this reason and the obvious fact that the system was limited to only one type of specimen, the results of this investigation must be considered only as trends and not as standard values.

However, for analysis of individual observations, the single sample technique is most useful in determining acceptable limits of deviation and in giving an approximation of the actual error involved. It also serves as an indicator to point out those cases to which no cause of error can be assigned yet which have results that are not compatible with the other observations. An example is given at the end of this chapter after the discussion of sources of error.

The temperature measurement technique contained the principal chance for error and all numerical results were a direct consequence of these values. In obtaining temperature drops across the interface and the temperature gradient, the absolute errors in individual readings were not important so long as these errors were uniform in all thermocouples. To minimize these errors, all thermocouples were manufactured by the same method and from the same spool of wire. All readings were made on the same potentiometer and referenced against the same standard cell. All thermocouples and thermocouple wire leads were the same length and similarly connected. The sensitivity of the potentiometer was $\pm .001$ millivolt or approximately $\pm 0.04^{\circ}\text{F}$ at the corrected mean gap temperature.

The temperature gradient and the interface drop were obtained by drawing the "best straight line" through a plot of the eleven readings of temperature vs. axial distance from the interface as shown in Figure III-C-1. Accuracy is considered doubtful for all Δt 's less than 2.0°F since line positioning could result in an error of $\pm 0.2^{\circ}\text{F}$ thus introducing unacceptable deviations.

Non-parallel heat flow was a second potential source of error. This could result from two effects: (a) non-uniformities in the heat path and (b) radiation losses in the radial direction. The non-uniform heat path is expected by the very nature of contact resistance and may possibly result from inhomogeneties in the metal. These latter can not be compensated for except where thermocouples are inserted. The thermocouple spacing and cementing material was designed to minimize any adverse effects. Any radial heat leakage from the stack that might affect the gradient would always be outward and thus have no influence on the relative trend obtained. Brunot and Buckland (8), and others, including the authors, have observed that the temperature gradients in both specimens were very nearly linear and also nearly equal, thus indicating that the transverse heat flow was negligible. For practical reasons obtaining a heat balance, especially while working in the vacuum system, was not seriously considered. All thermocouple holes were the same depth to insure the readings would be taken at the same distance from the vertical centerline of the stack should there have been a radial temperature distribution. In the majority of cases, all temperature readings fell along a straight line within the limits of position and thermocouple error. The linear extrapolation of the axial temperature gradient to the interface is considered to have been sufficiently accurate so that any error resulting from this extrapolation

was assumed negligible. In a similar experiment Weills and Ryder (35) made the following observations:

The errors associated with the experimental measurement of temperature, thermocouple location, thermal current and pressure are small compared with the variation due to asymmetrical heat flow caused by not having perfectly uniform loading over the cross section of all the joints and the variations due to changes in the metals themselves. Evidently the heat flow is nearly constant in any one axial path but varies somewhat from point to point over the joint area.

The radiation runs proved conclusively that the transfer of heat by radiation in this apparatus was negligible in comparison to that conducted through the metal or air. This is reviewed in detail in the Discussion of Results. The conductance reported represented the average value for the entire interfacial area computed at the mean of the two extrapolated metal temperatures at the interface and then corrected to 225°F. Since all specimens were identical in instrumentation this conductance comparison is considered valid.

By preloading each set of specimens, while hot, beyond the maximum experimental loadings, it is considered that all high spots were permanently deformed so as not to result in interference in subsequent tests. Thus it is hoped that the time effect on conductance has been eliminated and in fact no such variation was obtained when a specimen pair was left for a long period of time under identical conditions.

The value used for thermal conductivity, k , of the metal was supplied by the Aluminum Company of America (1) and was a computed value based on electrical resistance measurements at room temperatures. The estimated accuracy of this value is $\pm 5\%$. There remains the possibility that the value of k permanently changes with long time application of high

temperature in the aluminum. According to Bowden and Tabor (6) conductivity varies with pressure as given by the empirical expression $k_p = k_0 (1 + n \times 10^{-9} p)$ where k_p is the thermal conductivity at a given pressure p and k_0 is the thermal conductivity in the normal state. The variable n is 3.6 for silver and steel and most probably is of this order of magnitude for aluminum. A simple calculation shows that the greatest possible effect in this apparatus would have been approximately 2%. Bridgeman (7) obtained a value of the pressure coefficient of thermal conductivity for iron and copper at a load of approximately 2×10^5 pounds per square inch. For iron the value was -0.3% and for copper -9.0%. It is believed that aluminum will be intermediate to these two values. The maximum pressure during this investigation was of the order of 1.5×10^3 pounds per square inch and it is believed that the applicable value for aluminum would certainly not be greatly in excess of the 2% value above. This effect on the thermal contact conductance was neglected because its influence is small and no reliable values of pressure coefficient for aluminum were available.

One difficulty experienced was in obtaining a vertical stack alignment at the load cell under light loads. A rigidly attached cell would probably have been more accurate but was not available. However, since compatible results were obtained over repeated series of loadings and calibrations, the load values are considered to be consistent with the calibration used.

Further sources of error which are relatively insignificant were (a) the variation of coolant temperature during the time required for an observation, (b) the heat loss along the thermocouple wire and (c) the bi-metallic thermoelectric effect at the connector terminals. The latter connections were designed and located to insure that both connections for

each thermocouple lead would remain at the same temperature thus assuring no effect on the resulting reading from this extra junction.

An example of the single sample technique as applied to this investigation is given as follows for the equation:

$$h = \frac{k A}{\Delta t} \frac{dt}{dx}$$

At high pressures, where Δt becomes small and thus the controlling variable, i.e., $\Delta t = 2 \pm 0.2$ °F; $\frac{dt}{dx} = 240 \pm 5$ °F per foot; $k = 104 \pm 5$ BTU-foot per foot² °F; $A = 0.049 \pm 0.001$ Foot². Then the standard deviation from the mean value is given by the equation:

$$\left(\frac{\sigma_h}{h}\right)^2 = \left(\frac{\sigma_k}{k}\right)^2 + \left(\frac{\sigma_A}{A}\right)^2 + \left(\frac{\sigma_{\Delta t}}{\Delta t}\right)^2 + \left(\frac{\sigma_{\frac{dt}{dx}}}{\frac{dt}{dx}}\right)^2$$

where the σ 's are the standard deviations of the variables as assigned

above. $\left(\frac{\sigma_h}{h}\right)^2$ becomes approximately 0.011 or 10.5%. It is noted that

the temperature uncertainty contributes the 0.01 and the other variables influence only the third decimal place.

In the low pressure region, "apparent" contact pressure contains the largest (and also a variable) uncertainty. At 300 pounds per square inch and below, the maximum error is five percent.

V. Experimental Results

The results of the various runs are tabulated in Appendix B, Table B-1. This table records the run number, the load applied to the specimens, the "apparent" interface pressure, the temperature drop across the interface, $\frac{dt}{dx}$ (the temperature gradient), the mean temperature at the interface, the thermal contact conductance computed for each run, and the thermal contact conductance corrected to a mean interface temperature of 225°F. Since the metallic contact area at the interface is actually much less than the cross-sectional area of the specimens, the pressure is called "apparent" interface pressure. This "apparent" pressure is the total load applied, as measured by the load cell, divided by the cross-sectional area of the specimens.

Plots of thermal contact conductance corrected to 225°F. vs. "apparent" interface pressure to rectangular and semi-log scales are included as Figures B-1 through B-6.

The mean interface temperature was held in the neighborhood of 225°F. except for a few runs made at constant loads to obtain the variation of thermal contact conductance with mean interface temperature. Load was varied from no load to about 10,000 pounds, thus varying "apparent" interface pressure from zero to about 1400 pounds per square inch.

Tests were made on three sets of specimens as follows:

Specimens 1. Contact surfaces "optically" flat, i.e., flat enough to produce interference fringes when checked with an optical flat.

The mean value of roughness of these specimens was 9.7 microinches RMS, 7.4 microinches arithmetic average, with 110 microinches maximum peak-to-valley distance.

Specimens 2. Contact surfaces "optically" flat. These specimens

were prepared with a roughness intermediate to that of specimens 1 and 3 but were not utilized because of time limitations.

Specimens 3. Contact surfaces "optically" flat. The mean value of roughness of these specimens was 136 microinches RMS, 111 microinches arithmetic average, with 727 microinches maximum peak-to-valley distance.

Specimens 4. Tested with contact surfaces not optically flat but flat to within 0.0002 inches. The mean value of roughness during these tests was 67.8 microinches RMS, 56.2 microinches arithmetic average, with 432 microinches maximum peak-to-valley distance.

Specimens 4 were also tested with the contact surfaces "optically" flat. The mean value of roughness during these tests was 9.0 microinches RMS, 7.3 microinches arithmetic average, with 80 microinches maximum peak-to-valley distance.

A summary of the roughness measurements for all of the specimens is tabulated in Appendix B, Table B-4.

All of the runs showed that the thermal contact conductance was increased with an increase of "apparent" interface pressure. The rate of increase of thermal contact conductance with "apparent" interface pressure always remained constant or increased with an increase in pressure. No decrease in this rate was observed with any of the series of runs conducted.

Due to the extreme flatness and smoothness, i.e., small roughness, of specimens 1, the thermal contact conductance increased at such a rapid rate that instrumentation limitations prevented obtaining enough results for a quantitative evaluation.

Initially difficulty was experienced in obtaining satisfactory vacuum

data with specimens 3. It is believed that the stack became cocked, thus giving improper contact of the specimens and resulting in a wide scatter of data.

A comparison of the curves for specimens 4, flat and non-flat, showed that a marked increase of conductance was obtained by making the specimens "optically" flat. The roughness was different in each case, however it is considered that most of the increase in thermal contact conductance was a result of their increased flatness.

A comparison of the curves for specimens 4, flat, and specimens 3, and the limited data for specimens 1 indicate that the thermal contact conductance increases with a decrease of roughness. Insufficient data were taken to obtain a quantitative value of this variation, however the trend is definite. A comparison of the curves of specimens 4, non-flat, and specimens 3 gives much more striking evidence of the effect of flatness. Specimens 3 were much rougher than specimens 4, and, but for the effect of flatness, would be expected to have lower values of conductance. As the curves show, however, the conductances of specimens 3 were much greater than those of specimens 4 when non-flat.

The plots of thermal contact conductance vs. mean interface temperature for runs 169 through 173, Figure B-8, which were vacuum runs and for runs 138 through 140, Figure B-7, which were air runs indicates a direct variation of thermal contact conductance with mean interface temperature. It should be noted that these runs were over a limited temperature range and it is somewhat doubtful that the values should be extrapolated to cover a much wider range.

From the plots of thermal contact conductance vs. "apparent" interface

pressure mean values were obtained from the curves. These are tabulated in Appendix B, Table B-2. From these values $\frac{h_a}{h_T}$ and R were computed and tabulated in Table B-2. The values of $\frac{h_a}{h_T}$ are an indication of the percentage of the total heat being transferred which is conducted through the air. It is seen from Figure B-10 that the proportion of the total heat transferred across the interface by conduction through the included gas film increases somewhat with an increase of "apparent" interface pressure, reaches a maximum, then decreases with a further increase in pressure, and finally appears to reach a constant value. The magnitude of this variation seems to be more sensitive to roughness than to flatness.

VI. Discussion of Results

As described in the Introduction, heat is transferred across the contact interface by three methods as follows:

1. By conduction through the points of metallic contact,
2. By conduction through the air (or other included medium) film between the surfaces, and
3. By radiation.

Several investigators have made estimates of the proportion of the total heat which flows via each of the three paths but no reports of an experimental determination of the proportion could be found. Most of the estimates have been made by applying an analytical approach to experimental data on thermal contact resistance or conductance. Barzelay, Tong, and Holloway (2) state:

It appears that across the interface joints none of the three modes of heat transfer (namely metal-to-metal conduction, air film conduction, and radiation) has any predominance over another.

Keller (19) states:

Numerical calculations from known radiation constants, however, shows that actually radiation can account for only a very small, in fact a negligible, percentage of the total heat transfer.

The heat transfer which can be accounted for by metal-to-metal contact, therefore, while by no means negligible, still is only a minor part of the total.

. . . almost 98 percent of the radial conductivity in strip coils is due to gas film conduction, . . .

It should be noted that in Keller's work with strip coils, the radial heat flow corresponds to the axial flow in this work. Weills and Ryder (35) state:

In the pressure region beyond 10 psi there is no doubt that the larger fraction of heat flows through the metal contact areas.

Boeschoten states (5):

. . . most of the heat transfer takes place along the spots where the surfaces touch each other and that the transfer by the gas in the gap is relatively small.

The results of these investigations, like those of Keller, show that the amount of heat transferred across the interface by radiation is negligible. The amount transferred by this method was less than 10 percent at the lowest loads (smallest conductances) and immediately dropped off to less than 1 percent at very light loads. The value of heat transferred by radiation used in obtaining these percentages is actually a gross exaggeration of what is believed to be the actual value as will be discussed below. These investigations also showed that the proportion of heat transferred through the gas film was of the same order of magnitude as that transferred through the metal. The actual proportion varied with roughness and flatness of the specimens and with "apparent" interface pressure. Values of from about 0.15 to about 0.85 were observed. It should be noted that the proportion of heat flowing by conduction through the air film, and through the metal, tended toward a constant value at high "apparent" interface pressures. At very light loads the form of the computations involved the difference between two conductances of very nearly the same value, thus giving a large possibility of error and unreliable results. For this reason, a quantitative comparison cannot be made with the results of Keller, who made his investigations in the region of 10 psi "apparent" interface pressure.

In considering the radiation runs several factors must be taken into account. No radiation shields were used, thus giving the possibility of re-radiation to the lower (cooler) specimen from the upper (hotter) specimen via the jar walls and giving a larger value of conductance as a

result of radiation across the interface than actually existed. The temperature difference across the interface was greater by nearly an order of magnitude than any of the other temperature differences observed. Since the quantity of heat transferred by radiation is dependent upon this difference, this effect would result in a larger value of conductance resulting from radiation than would be experienced during an air or vacuum run. In order to maintain the alignment of the specimens in the vacuum jar it was found necessary to provide a guide during the radiation and vacuum runs. A Teflon ring was used for this purpose and while Teflon is an excellent heat insulator it is not perfect; therefore, heat will be transferred through the Teflon, thus giving a slightly higher value of conductance for the radiation and vacuum runs. When the specimens are in contact a portion of the "apparent" contact surface is actually in contact. Any area which is in contact is thus unavailable for radiating, and again the conductance indicated by the radiation runs is high compared to the actual conductance resulting from radiation during air and vacuum runs. As was pointed out, all of these effects would make the actual value of conductance from radiation smaller than indicated; however, the value observed was found to be negligible so it has merely been made "more negligible."

As stated in the Introduction, one of the purposes of this investigation was to determine an actual area of metallic contact at the interface by utilizing the results of both vacuum and air runs. An actual area of contact was not found as discussed below; however, a shape factor called the "effective" metallic contact ratio was determined. This ratio should prove to be useful in predicting the effect of using various gases

as included media. The variation of R with "apparent" interface pressure is shown in Figure B-9. By substituting the thermal conductivity of the gas in question into the equation of Appendix C, the new thermal contact conductance can be predicted as shown by the example of Appendix C. To use the "effective" metallic contact ratio for these predictions it is necessary to assume that the ratio $\frac{s_m}{s_a}$ does not vary from one gas to another. This is not entirely true since this factor will vary somewhat with the conductivity of the included medium. It is considered, however, that as long as the conductivity of the medium is at least an order of magnitude removed from that of the metal, that no appreciable error will result in the predictions made. It would be desirable to make predictions of the actual metallic contact area from the vacuum runs; however, some of the factors which influence thermal contact conductance during vacuum runs (namely roughness and flatness) are so illusive of measurement and designation that it is considered that it is not practicable at this time to make quantitative predictions of the influence of these parameters. It is possible to set up empirical relations describing the variation of conductance with "apparent" interface pressure. This would be an indication of the contact area but the results would be meaningless quantitatively unless the values of roughness and flatness could be duplicated.

When the values of "effective" metallic contact ratio are examined it is found that if the factor $\frac{s_m}{s_a}$ is assumed to be unity, the resultant "metallic contact areas" are very unrealistic from the allowable stress point of view. Values of "metallic contact area" of the order of 10^{-3} square inches would be indicated from the values of R listed in Appendix

as included media. The variation of R with "apparent" interface pressure is shown in Figure B-9. By substituting the thermal conductivity of the gas in question into the equation of Appendix C, the new thermal contact conductance can be predicted as shown by the example of Appendix C. To use the "effective" metallic contact ratio for these predictions it is necessary to assume that the ratio $\frac{s_m}{s_a}$ does not vary from one gas to another. This is not entirely true since this factor will vary somewhat with the conductivity of the included medium. It is considered, however, that as long as the conductivity of the medium is at least an order of magnitude removed from that of the metal, that no appreciable error will result in the predictions made. It would be desirable to make predictions of the actual metallic contact area from the vacuum runs; however, some of the factors which influence thermal contact conductance during vacuum runs (namely roughness and flatness) are so illusive of measurement and designation that it is considered that it is not practicable at this time to make quantitative predictions of the influence of these parameters. It is possible to set up empirical relations describing the variation of conductance with "apparent" interface pressure. This would be an indication of the contact area but the results would be meaningless quantitatively unless the values of roughness and flatness could be duplicated.

When the values of "effective" metallic contact ratio are examined it is found that if the factor $\frac{s_m}{s_a}$ is assumed to be unity, the resultant "metallic contact areas" are very unrealistic from the allowable stress point of view. Values of "metallic contact area" of the order of 10^{-3} square inches would be indicated from the values of R listed in Appendix

B, Table B-2. With loads of say 5,000 pounds this would indicate stresses at the points of contact of 5×10^6 pounds per square inch which obviously the aluminum cannot support. There are several possible explanations for this. One source of difference is undoubtedly due to the "spreading resistance" or "spreading conductance" concept as described by Weills and Ryder (35):

"Spreading resistance" or "spreading conductance" . . . concept that the lines of flow of heat must fan or spread out after passing through a contact area which is smaller in size than the boundary of the solids in contact. It is a measure of the fact that not all of the volume of the solids in contact is equally available for the conduction or flow of heat.

This effect is analogous to the "constriction resistance" observed by Holm (15) with electrical contacts.

. . . the current lines of flow are bent together through narrow areas, causing an increase of resistance compared with the case of a fully conducting, apparent, contact surface. This increase of resistance we call the constriction resistance.

Holm has developed a form for determining the actual metallic area of contact as follows:

. . . plane contacts would give contacts with merely elastic yielding. But the waviness sets a limit to this development. Even in a new plate contact many contact spots yield plastically so that the mean pressure \bar{p} satisfied the following conditions:

$$\bar{p} = 0.5 H \text{ to } 0.8 H \text{ or } P = 0.5 H S_b \text{ to } 0.8 H S_b$$

Note: \bar{p} = "apparent" interface pressure

P = Total load applied

H = Meyer hardness

S_b = "Actual" metallic contact area.

It should be noted that the hardness used by Holm was the Meyer hardness.

This hardness is defined by formula as follows (26):

$$P_m = \frac{L}{\frac{\pi d^2}{4}} = \frac{4L}{\pi d^2}$$

where L = load in kg

d = diameter of indentation in millimeters

(P_m = number representing the mean pressure supported by the metal-Meyer hardness number)

The reason for using this hardness is expressed by Cetinkale and Fishenden

(10) as follows:

In contact problems, Meyer hardness must be used in preference to other hardnesses since it gives the projected area of the solid spots, which is the smallest area exposed to flow.

Values of Meyer hardness for the aluminum used in the specimens investigated are listed in Appendix B, Table B-3. These values of hardness are for room temperature with a short time load.

Rearranging Holm's expression for the "actual" metallic contact area, it is seen that the metallic contact area is directly proportional to the applied load and inversely proportional to the Meyer hardness. For the time being it will be assumed that the hardness is a constant since all of the specimens were taken from the same bar. This leaves the contact area directly proportional to the applied load. To find how the contact area increases it is assumed that the contact area increases partially by enlarging the area of contact at the points of contact and partially by making new points of contact. As the load is further increased, these new points of contact may expand as the original points and the overall effect would be contact at more and larger points. Since the "spreading conductance" is caused by a throttling action through the points of contact, it follows that the "spreading conductance" should increase, thus allowing more heat to flow through the metallic points of contact. Also with larger actual metallic contact area more heat should flow through the metal. While it is seen from the plots of the vacuum runs that the conductance due to conduction through the metal does increase with pressure, an examination of Figure B-10, Appendix B, shows that the

percentage of total heat transferred by conduction through the air initially increases with an increase in pressure. This would indicate that the mechanism of increasing contact area is primarily an increasing of the number of points in contact rather than a large increase in area of the existing points of contact. If this mechanism is assumed, it is seen that while the metallic contact area increases, so does the "spreading resistance" with a resultant decrease of "spreading conductance." The overall effect is that the percentage of heat transferred by conduction through the metallic contacts decreases. As the pressure increases further apparently the mechanism of contact shifts to that first postulated, i.e., an increase of area of the existing contacts. The mechanism then apparently shifts back to an increase in area due to new small points of contact, possibly caused by a "splintering" effect in the existing points of contact. The effect of the small points of contact is not as pronounced in this case as at lower pressures and the overall effect is a nearly constant proportion of the heat being transferred by conduction through the gaseous film. Bowden and Tabor (6) have related the area of contact to the number of contact points as follows:

The value of conductance must depend both upon the size of the metallic bridges and their number. Since the spreading resistance of each bridge is inversely proportional to its diameter, and the area of contact is proportional to the square of the diameter, it follows that, for a given conductance the area of contact is inversely proportional to the number of bridges. We do not know this number with any certainty, though in the case of flat surfaces it is clear that the number of legs on which they rest cannot be less than 3. Experiments suggest in fact, that the number of points of contact is greater than this.

In addition to the "spreading resistance" it is possible that a further resistance may be present due to the oxide film on the contact surfaces. However, according to Weills and Ryder (35):

Except at very low pressures the oxide resistance at the joint appears to account for only a small part of the total resistance.

Probably the dominant reason that the "effective" metallic contact ratio is not a realistic area factor lies in the invalid assumption that $\frac{s_m}{s_a}$ equals unity. This factor will be greater than unity and it appears that values of the order of 100 to 1000 would be more realistic. The assumption that this factor is unity is equivalent to the assumption that the equipotential lines are always horizontal, particularly near the interface. Actually this is true at some distance from the interface but is not at all true near it. Figure VI-1 illustrates a probable equipotential configuration near a point of contact during a vacuum run,

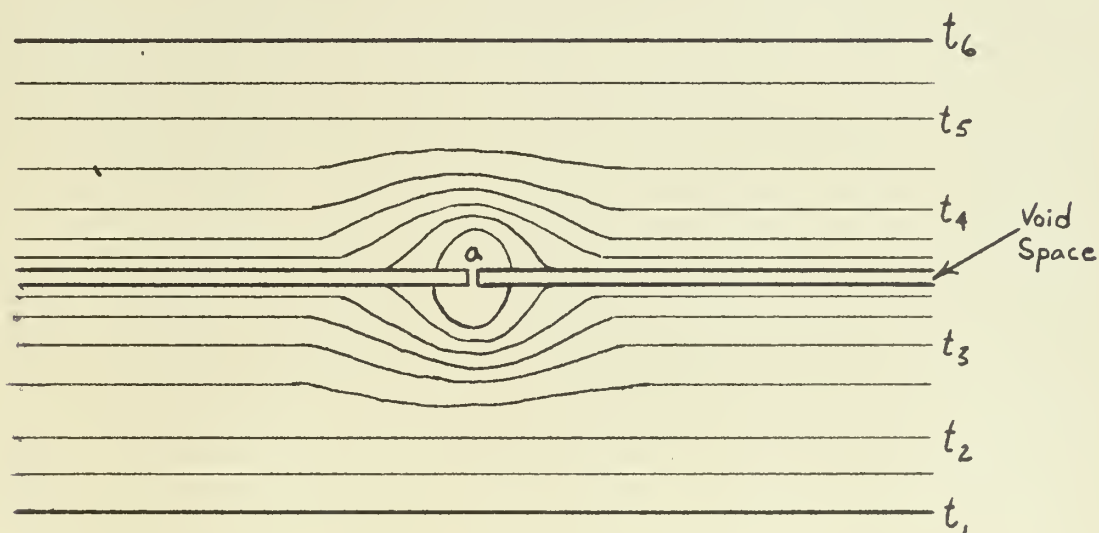


Figure VI-1

where a is a point of contact and the temperature increases from t_1 to t_6 .

The effect of time on the thermal contact conductance apparently is negligible. This does not mean that conditions are not changing. On the

contrary, it is believed that several conditions are changing which somewhat compensate for each other. As pointed out by Cetinkale and Fishenden (10) the Meyer hardness decreases with time.

It was found, using a Rockwell hardness testing machine, that, up to at least 24 hours

$$H = H_0 (1 - \Omega \log_e 180 \tau) \text{ for } \tau > \frac{1}{180} \text{ hr.}$$

where H and H_0 are the Meyer hardness for τ hours and $\frac{1}{180}$ hour application of the load respectively, and Ω is a constant.

There appears to be a wide variation in the results reported by various investigators in this field. Keller (20) mentions some of the reasons for this:

Discrepancies in results of investigators point to variation in character of surface roughness not indicated by RMS roughness figures. Not merely RMS roughness but more especially the height of the highest peaks of the surface above the mean level which largely determines the thermal conductance through the air film between the surfaces.

It was found that the flatness or waviness of the specimens was a very prominent factor in thermal contact conductance and since this factor is so difficult to describe accurately it is believed that this may have caused a large portion of the disagreement among the various investigators. Actually few of the investigators specify the flatness of the specimens which they used.

The limited investigation of the variation of thermal contact conductance with mean interface temperature made showed an increase with temperature, which is consistent with observations of all others who have investigated the variation with this parameter. This variation was observed only at single loads and about a single temperature but according to Barzelay, Tong, and Holloway (3):

For a given pressure increment the percentage increases of conductance is about the same for all interface temperatures. . . . it was found that the percentage rise (of conductance with a rise of mean interface temperature) is of about the same order of magnitude at higher pressure levels as at the low pressure level.

Some of the investigators in this field have reported a linear variation of thermal contact conductance with "apparent" interface pressure while others have reported exponential or power variation. Both were observed, depending upon the "apparent" interface pressure and the roughness and flatness of the surfaces. This gives further evidence for stating that variations among the several investigators may differ because of variations in flatness.

VII. Conclusions and Recommendations

Conclusions

1. The proportion of the total heat transferred across the interface by radiation is negligible.
2. The proportion of the total heat transferred across the interface by conduction through the included gas film increases somewhat with an increase of "apparent" interface pressure, reaches a maximum, then decreases with a further increase in pressure, and finally appears to reach a constant value. The magnitude of this variation seems to be more sensitive to roughness than to flatness.
3. Thermal contact conductance was observed to vary linearly with "apparent" interface pressure in some cases, and with a power of the pressure in others. This variation is believed to be determined by roughness, flatness, and "apparent" interface pressure.
4. A shape factor called the "effective" metallic contact ratio was computed for the specimens tested which should prove useful in predicting quantitatively the effect of various included media with these specimens.
5. The thermal contact conductance always increases with an increase of "apparent" interface pressure, other variables being held constant. The rate of increase always remains the same or increases with pressure at least to the limits observed.
6. Thermal contact conductance decreases with an increase in roughness of the contact surfaces.
7. Thermal contact conductance increases with the degree of flatness of the contact surfaces.

8. Thermal contact conductance increases with an increase of mean interface temperature.

Recommendations

It is recommended that:

1. This project be continued with some refinements being made in the equipment. The principal improvement can be seen to be a more accurate method for locating thermocouples. Use of X-ray photography or a smaller specimen with a hole drilled all the way through to accept a butt welded couple are two suggested methods for improvement. In addition, smaller specimens would allow the use of higher pressures with the existing equipment. A more positive means of fixing the position of the top plate would result in greater accuracy in alignment of the test stack. Use of a controlled temperature coolant could give an appreciable decrease in the time required between readings plus more accurate control of the mean temperature.

2. An investigation be made using other included media, both gaseous and solid, and using test specimens of other materials and roughnesses. These parameters should be tested with vacuum runs so that the effects of included media can be compared with runs where essentially all of the heat is transferred by conduction through the metallic contact. When using gaseous media other than air, predict the conductance using the values of "effective" metallic contact ratio reported herein and check the results.

3. An investigation be made with a potential field plotting method to check the results of this investigation if possible.

4. An investigation be made toward developing a suitable means for specifying flatness of surfaces, particularly in the range between

0.0001 inch and "optically" flat. One possibility suggested is "contour mapping" using a sensitive air gauge.



Figure A - 1 General Equipment Layout, Air Run

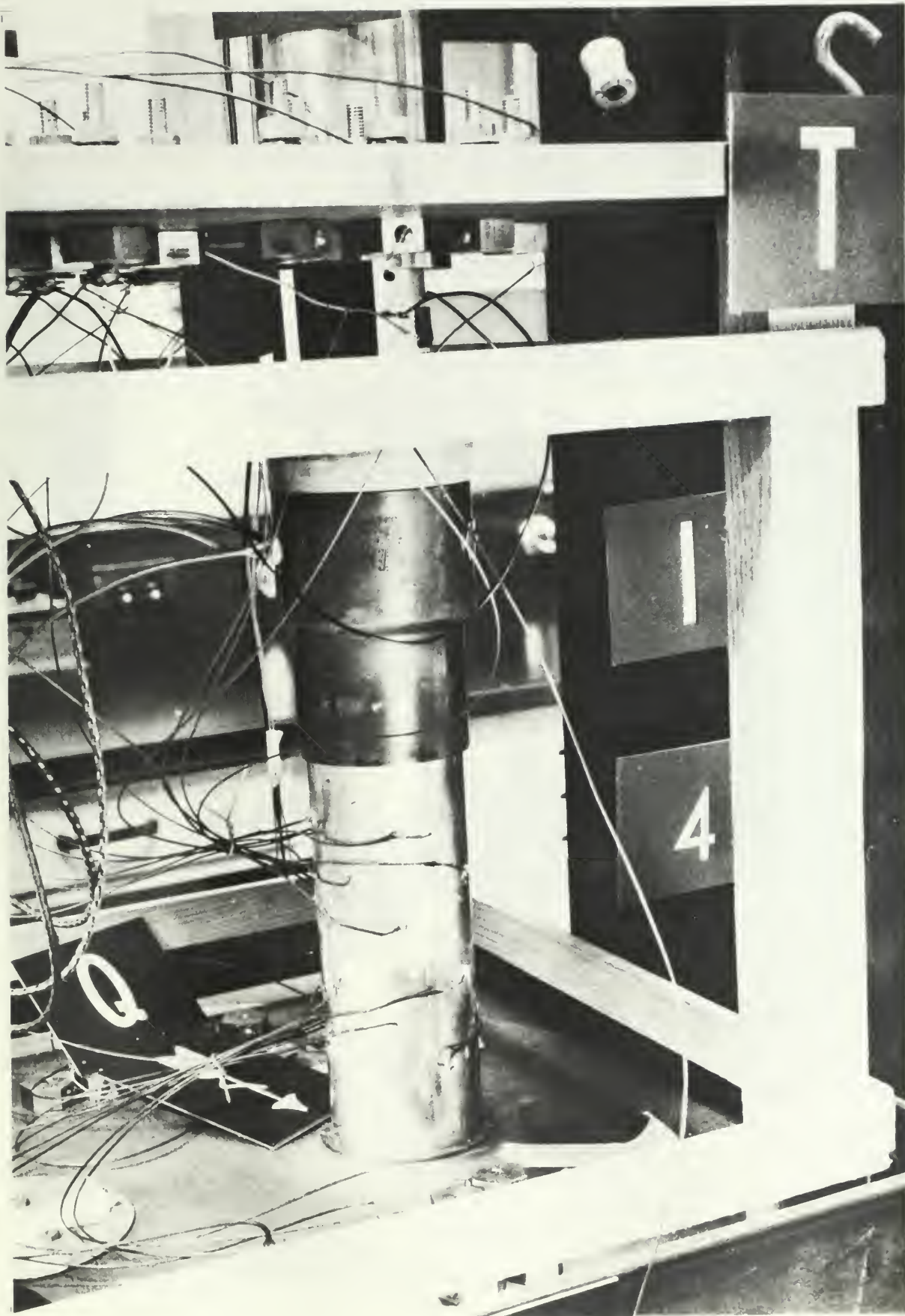


Figure A-2

Specimen Stack

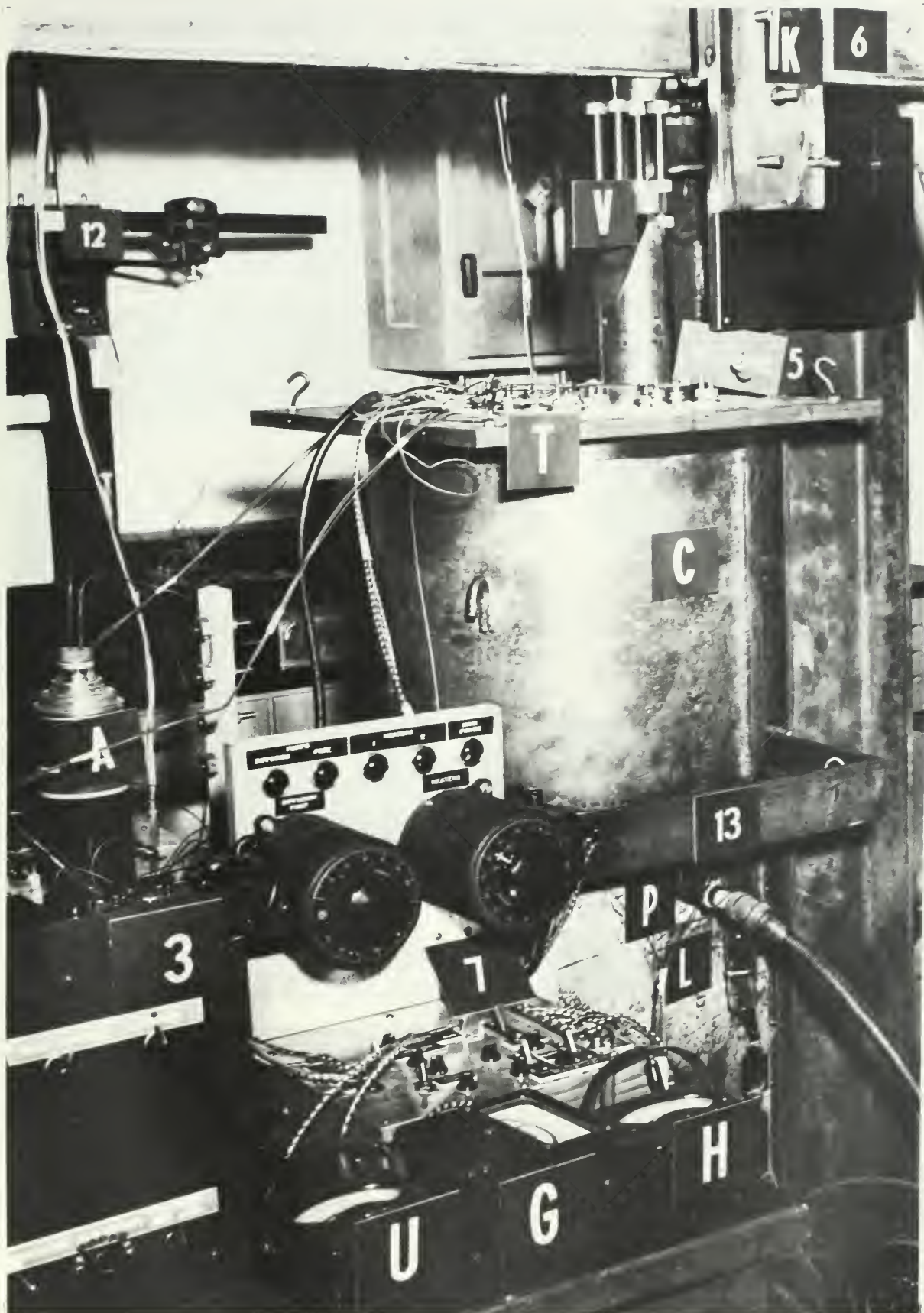


Figure A - 3

Equipment, Vacuum Run



Figure A - 4 Equipment, Radiation Run

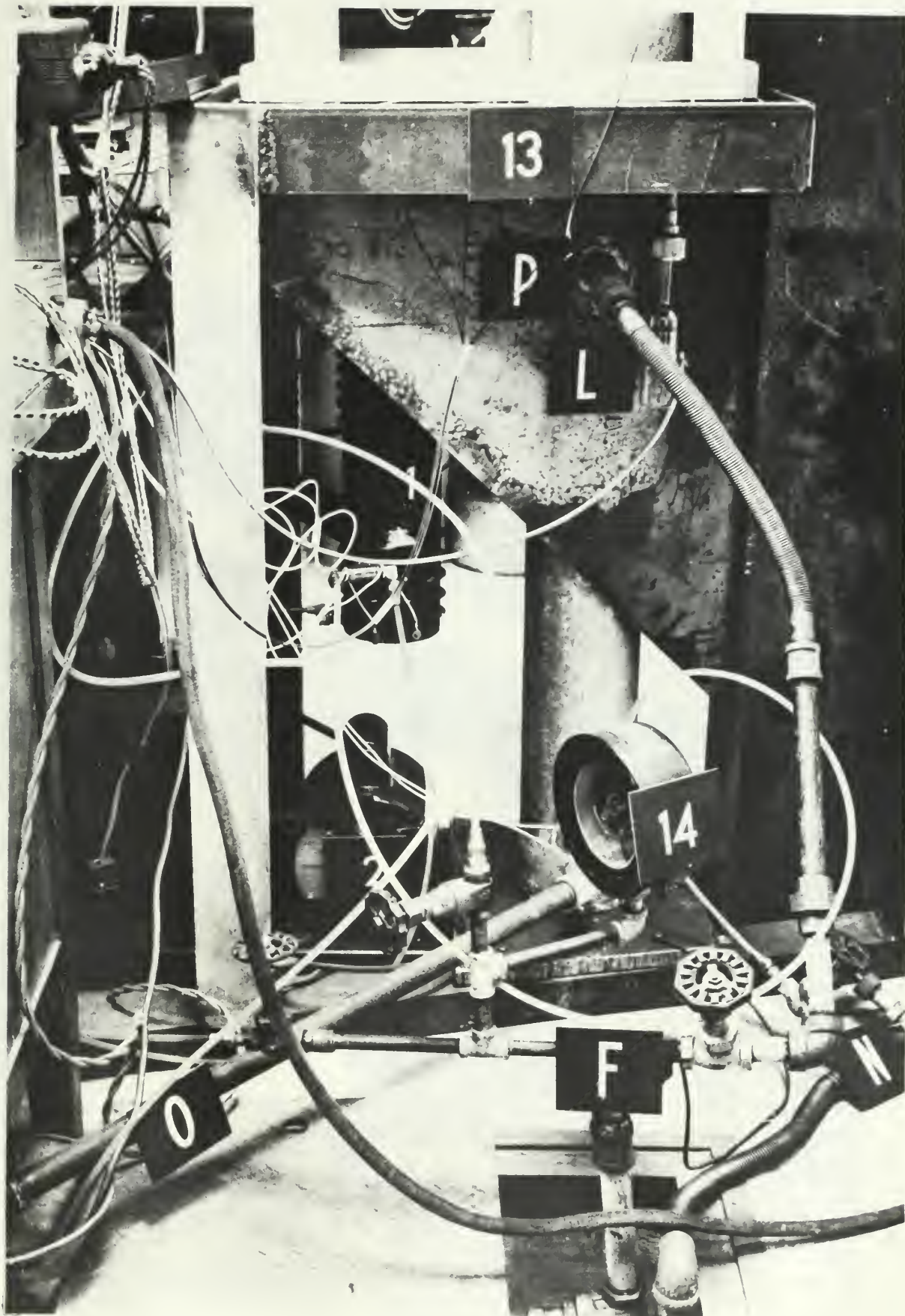


Figure A - 6

Equipment, Plumbing

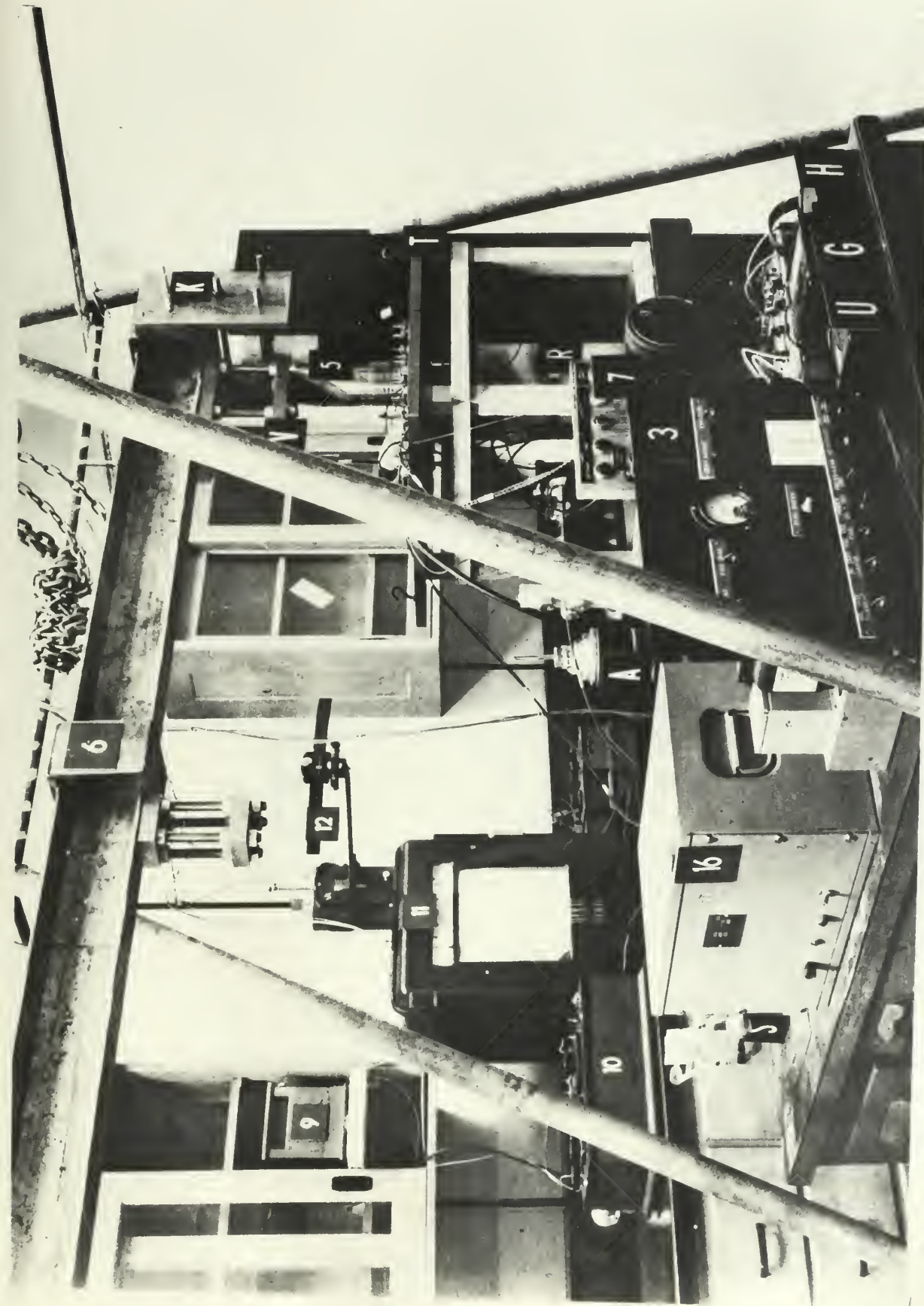

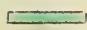

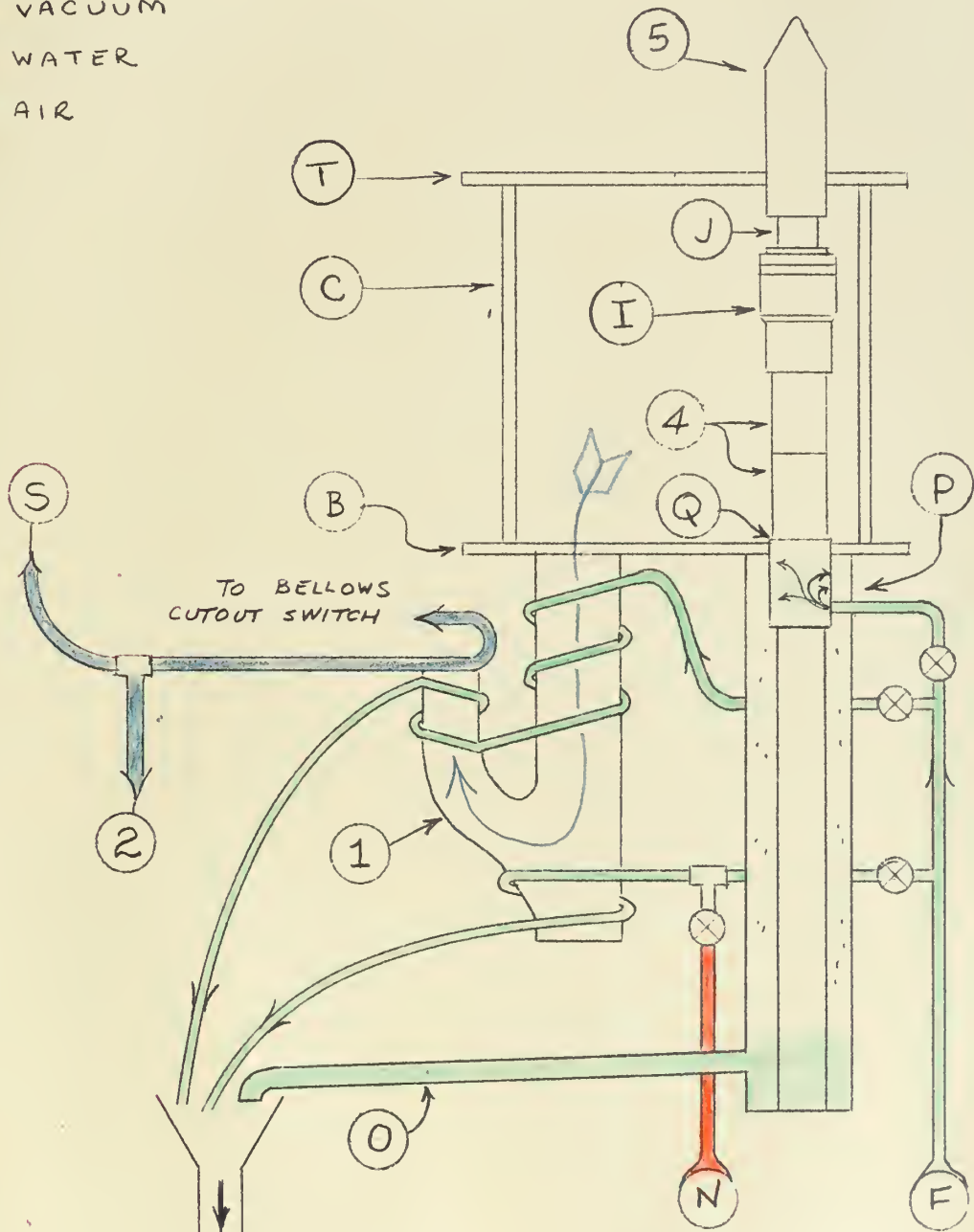


Figure A-7 General Equipment Layout, Air Run

SCHEMATIC OF VACUUM, WATER AND AIR SYSTEMS

 VACUUM
 WATER
 AIR



 SYMBOLS USED IN "DESCRIPTION OF EQUIPMENT" (CHAPTER II)
 SEE FIG A-15

Figure A-8

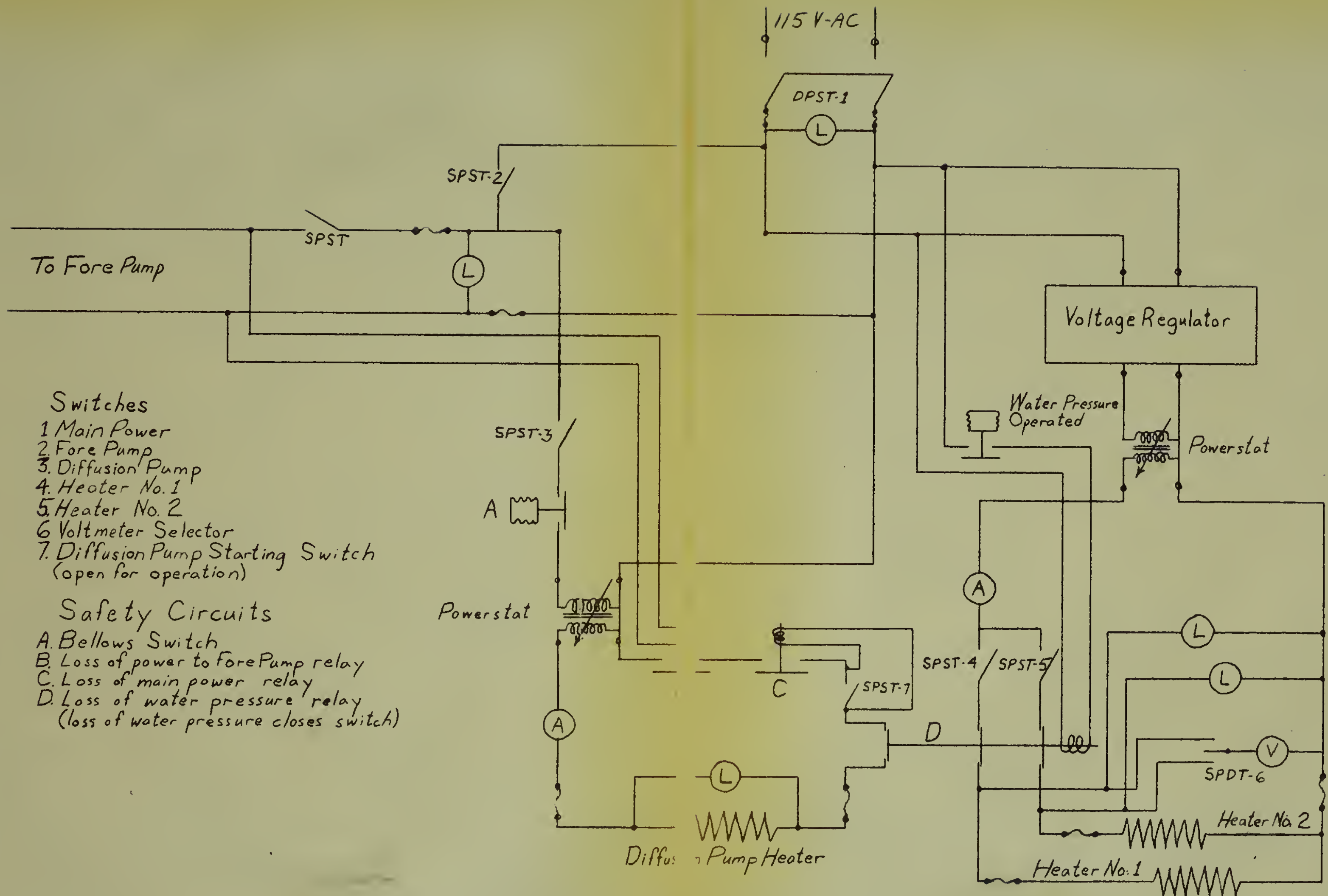
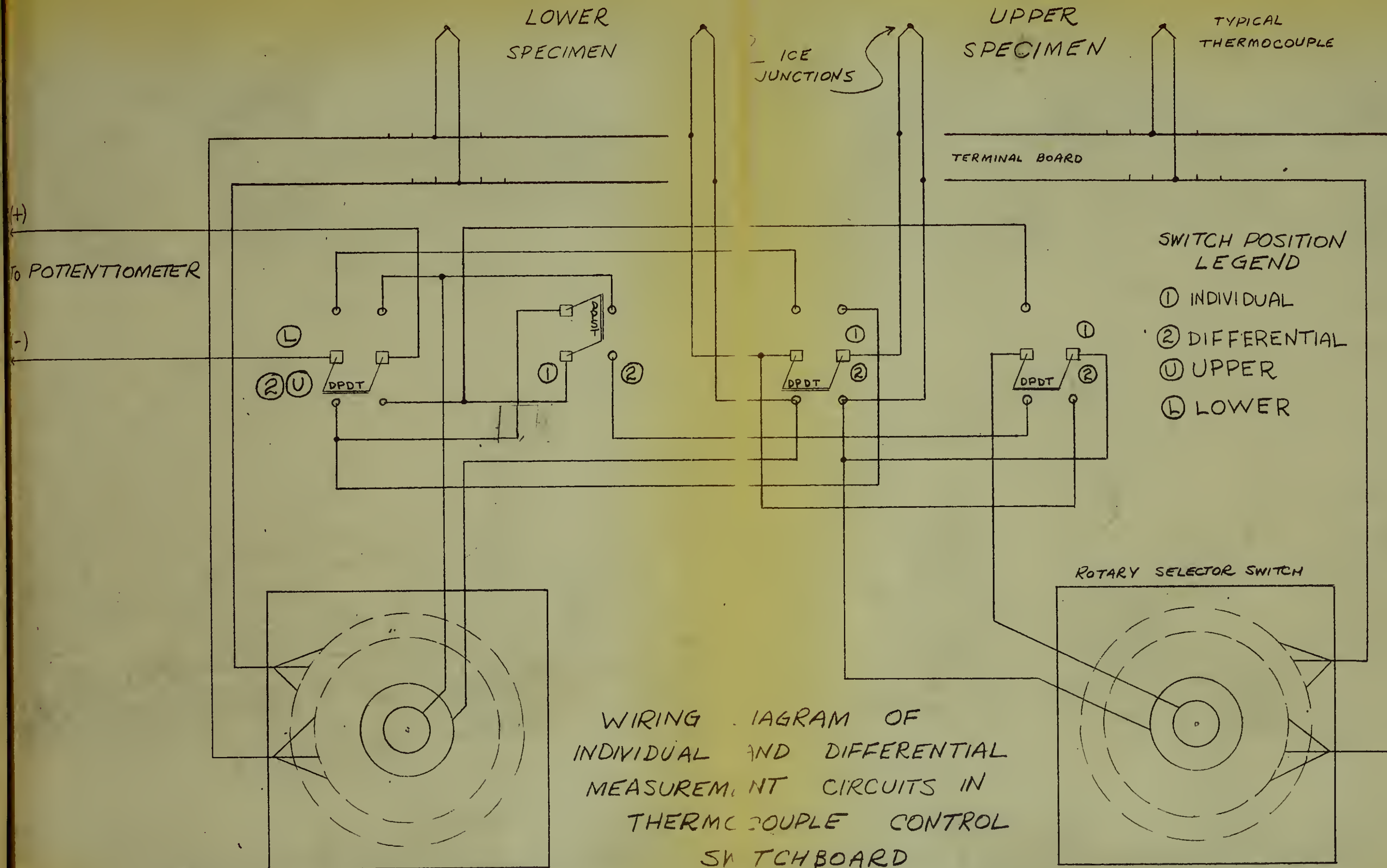
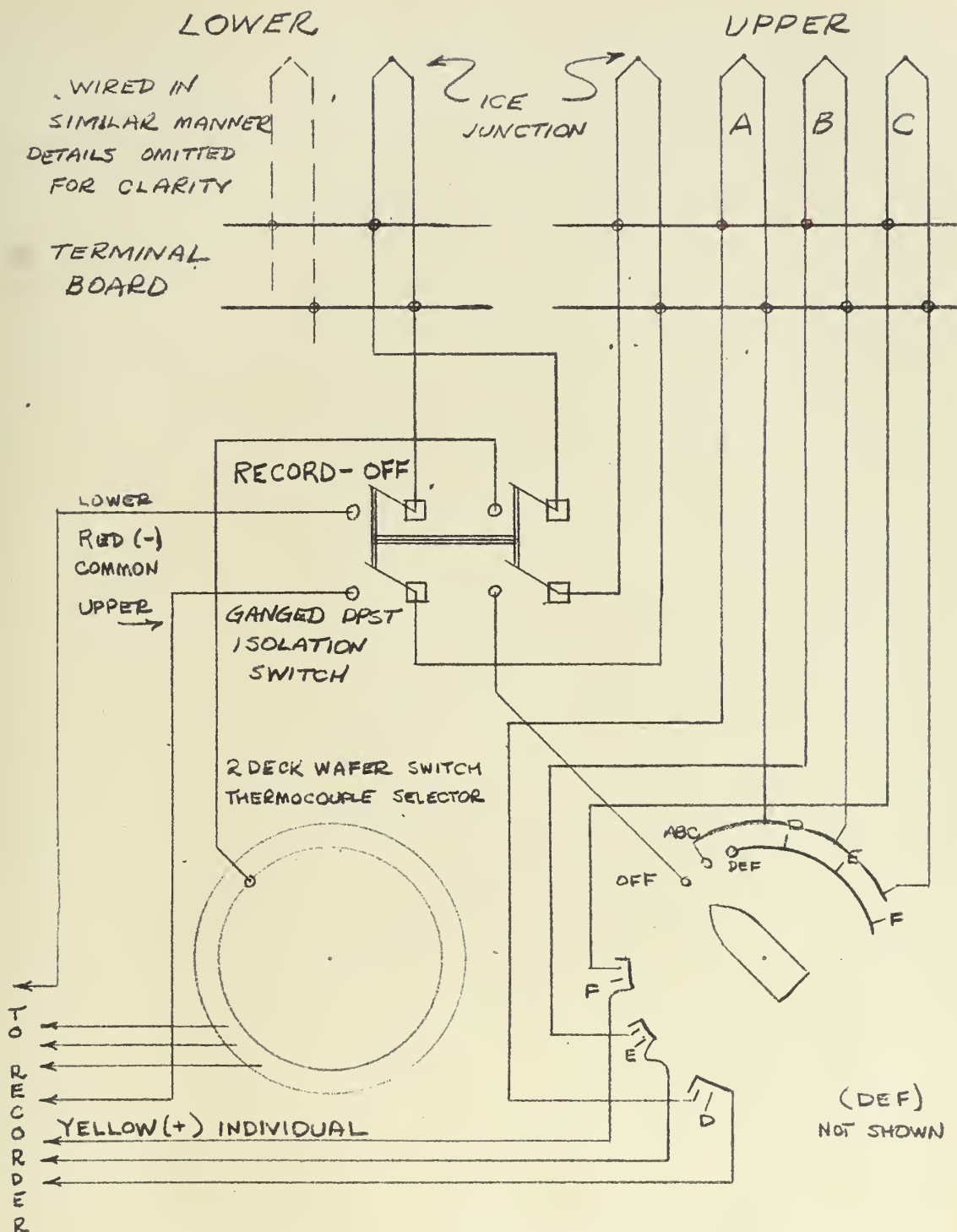


Figure A-9 Electrical Wiring Schematic



WIRING DIAGRAM OF
INDIVIDUAL AND DIFFERENTIAL
MEASUREMENT CIRCUITS IN
THERMOCOUPLE CONTROL
SWITCHBOARD

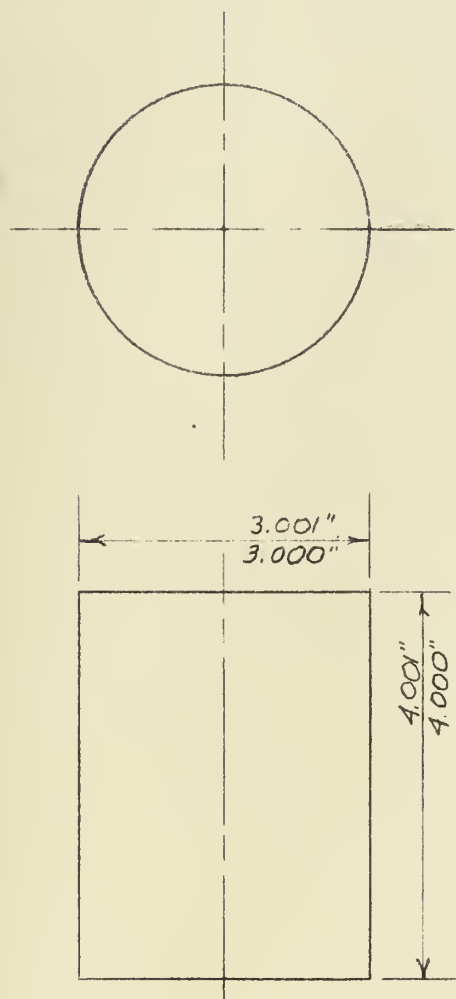
Figure A-2



PARTIAL WIRING DIAGRAM FOR
POTENTIOMETER RECORDER CIRCUIT
IN THERMOCOUPLE CONTROL SWITCHBOARD

Figure A-11.

MATERIAL: 6061 ALUMINUM ALLOY



THERMOCOUPLE LOCATION SPECIFICATIONS

SEQUENCE NUMBER	DISTANCE FROM TEST SURFACE	✕ SPACING BETWEEN HOLES
1	0.250"	
2	0.500"	100°
3	0.750"	"
4	1.000"	"
5	1.250"	"
6	1.500"	"
7	1.750"	"
8	2.000"	"
9	2.250"	"
10	2.500"	"
11	2.750"	"

NOTES:

1. USE #50 DRILL
2. ALL HOLES 1.25" DEEP
3. FACES PARALLEL TO WITHIN 0.0002"
4. TEST SURFACE FLAT TO APPROX. 100 μ in.

TEST SPECIMEN AND THERMOCOUPLE SCHEDULE

Figure A-12

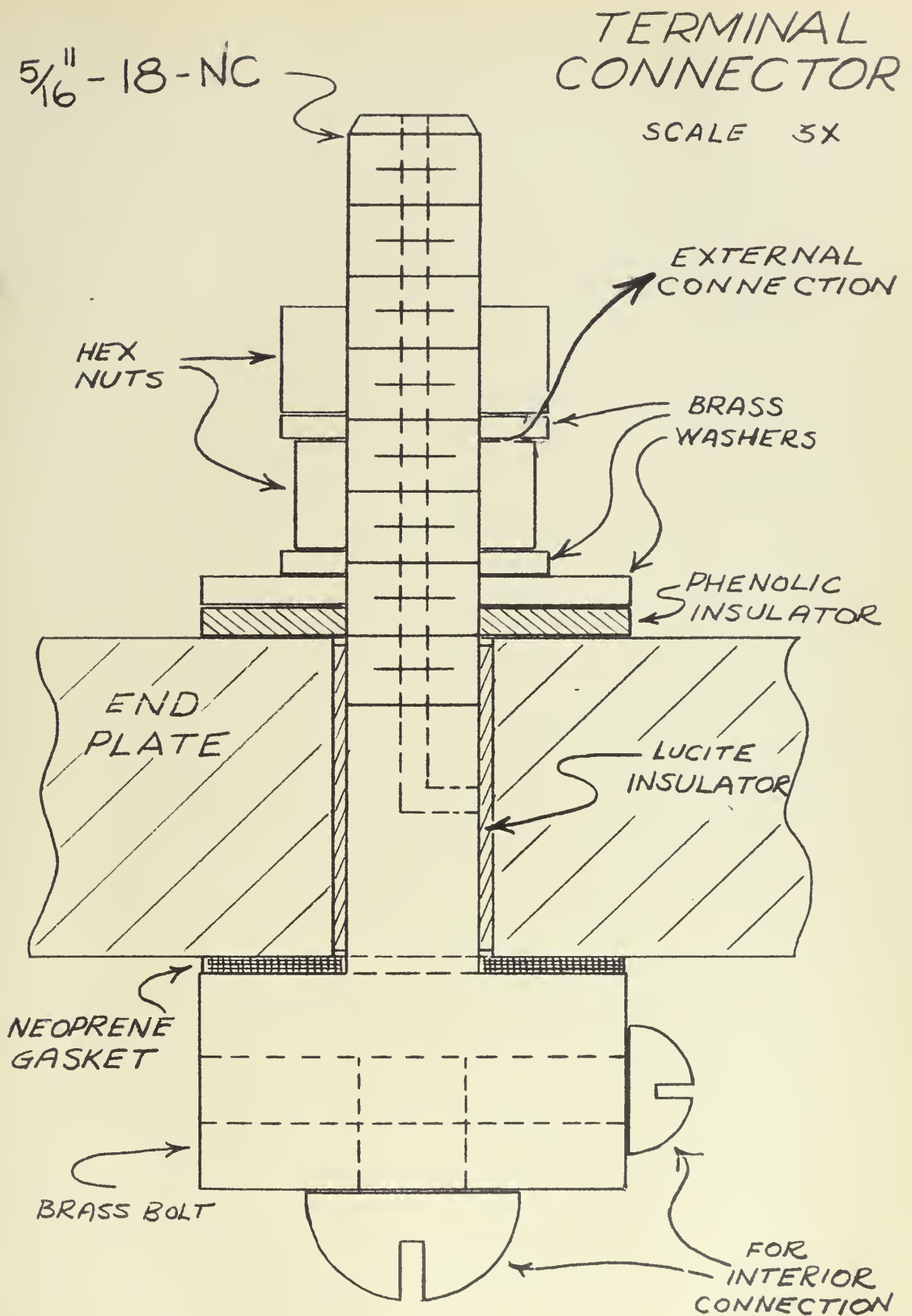


Figure A-13

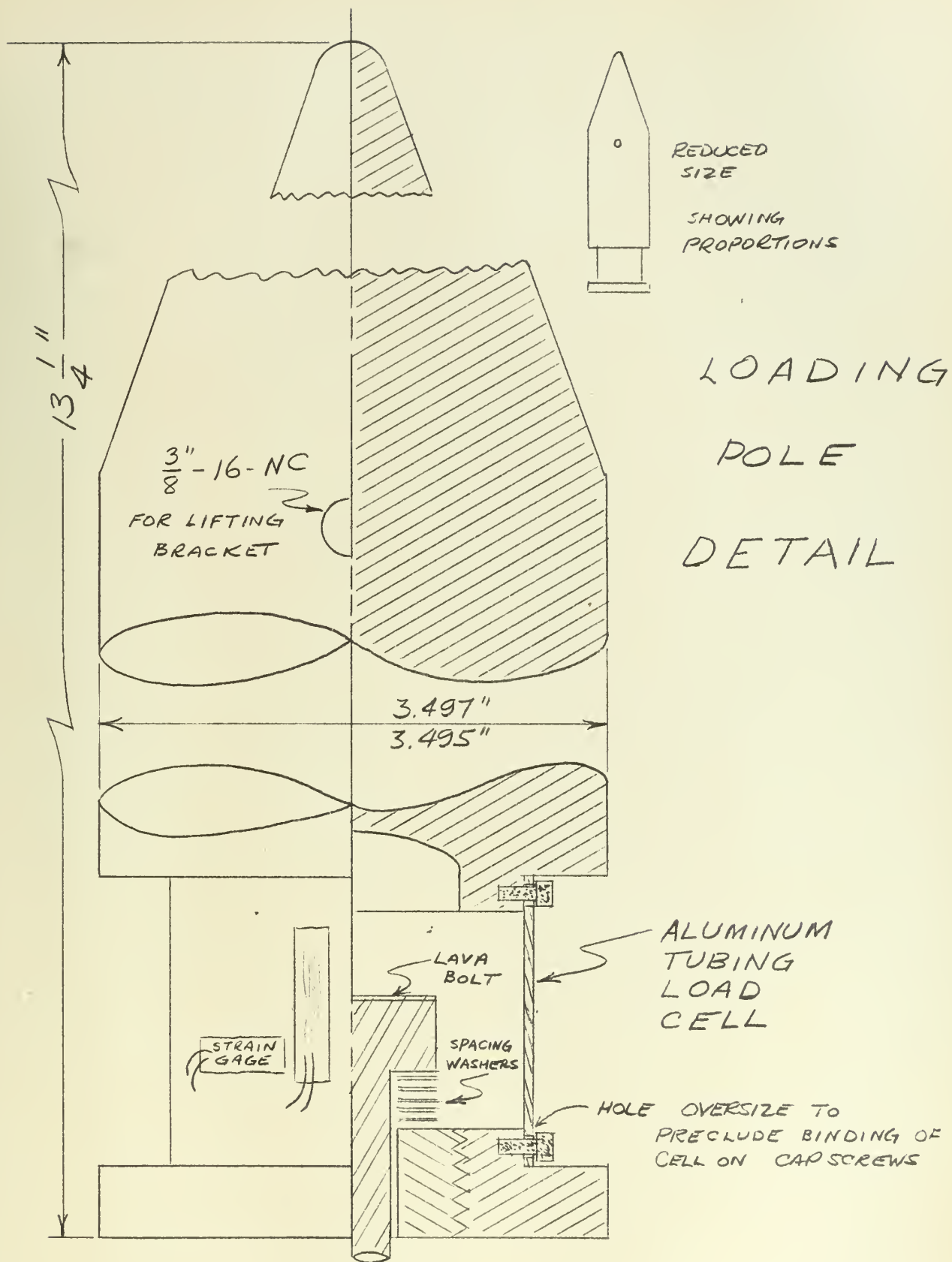


Figure A-14

EQUIPMENT SYMBOLS

1. Diffusion Pump	E. A-Frame
2. Fore Pump	F. Water Supply
3. Ionization Gauge Control	G. Heat Source Ammeter
4. Test Specimens	H. Heat Source Voltmeter
5. Loading Pole	I. Heating Head
6. Loading Arm	J. Load Cell
7. Power Control Switchboard	K. Pivot Plates
8. Thermocouple Control Switchboard	L. Ionization Gauge Tube
9. Temperature Galvanometer	M. Pirani Tube
10. Precision Potentiometer	N. Air Supply
11. Potential Recorder	O. Drain Connection
12. Leak Detector Galvanometer	P. Water to Cooling Head
13. Load Machine	Q. Cooling Head
14. Water Safety Switch	R. Insulating Jacket
15. Strain Indicator	S. McLeod Gauge
16. Voltage Regulator	T. Top Plate
A. Ice Junction	U. Diffusion Pump Heater Ammeter
B. Bottom Plate	V. Loading Plate
C. Vacuum Jar	W. Lifting Bracket
D. Weight Hanger	X. Screw Jack

Figure A-15

TABLE B-1 -- RUN DATA

Run	Pressure *	Δt	$\frac{dt}{dx}$	Mean Temp Interface	Observed h	h Corrected to 225 °F
	lb/in. ²	°F	°F/ft	°F	BTU/hr. ft ² °F	BTU/hr. ft ² °F
Vacuum Runs - Specimens 4, Non-Flat						
1	248.0	55.1	232.3	354.8	438.5	299.9
1A	244.4	57.1	222.7	253.2	405.6	284.3
2	536.6	28.9	232.8	235.4	837.9	745.7
3	737.4	21.9	238.1	231.4	1130	1053
4	888.8	17.1	237.1	231.6	1442	1341
5	976.5	16.4	235.2	230.7	1491	1402
6	1064	13.4	245.8	232.4	1908	1757
7	1107	13.5	233.3	226.2	1797	1779
8	1186	10.5	240.0	225.6	2377	2363
9	1360	7.5	242.9	223.8	3368	3412
10	1153	11.8	235.7	226.7	2077	2040
11	1231	10.9	239.0	225.4	2280	2171
12	1303	11.1	233.3	225.4	2186	2175
13	1371	9.2	233.8	225.3	2643	2635
14	1308	9.7	236.2	225.8	2532	2512
15	1233	10.0	238.1	226.6	2477	2435
16	1163	11.8	236.2	227.2	2082	2034
17	1081	13.8	234.7	228.2	1769	1709
18	990.6	15.4	240.0	229.3	1621	1546
19	919.9	17.4	235.7	230.4	1409	1329
20	852.0	19.2	234.7	230.9	1271	1191
21	778.5	21.9	232.8	232.6	1105	1015
22	716.2	26.5	232.3	233.5	911.8	829.7
23	689.3	27.1	234.2	235.0	898.9	803.6
24	610.1	28.2	240.0	235.5	885.2	786.9
25	506.9	31.5	244.3	230.2	806.7	762.3
26	444.6	40.4	247.7	244.0	637.7	508.9
26A	431.9	39.5	241.4	233.4	635.6	579.0
27	369.6	57.2	234.2	255.1	425.8	320.0
28	301.7	58.4	228.5	255.2	407.0	276.8
29	282.2	51.4	230.4	251.8	466.2	313.8
30	51.9	165.6	197.8	306.6	124.2	16.6
31	46.7	163.4	200.2	307.7	127.4	16.7
32	813.8	17.1	238.8	231.8	1452	1348
33	813.8	16.4	239.0	231.6	1515	1409

* Pressure is "apparent" interface pressure

Run	Pressure *	Δt	$\frac{dt}{dx}$	Mean Temp Interface	Observed h	h Corrected to 225 °F
	lb/in. ²	°F	°F/ft	°F	BTU/hr. ft ² °F	BTU/hr. ft ² °F
34	813.8	17.2	238.6	232.5	1442	1332
35	813.8	17.3	237.6	230.6	1428	1344
37	813.8	16.9	237.8	233.0	1463	1339

Air Runs - Specimens 4, Non-Flat

38	41.0	54.4	233.8	250.9	447.0	270.4
39	36.8	55.1	227.8	249.2	430.0	271.3
40	36.8	56.1	224.9	249.7	417.0	259.8
41	117.7	43.0	220.8	258.5	534.1	261.2
42	139.3	37.7	224.6	236.9	619.7	507.5
43	163.0	36.1	223.7	234.2	644.5	554.3
44	192.8	33.7	226.3	231.0	698.5	634.3
45	236.5	33.4	221.5	231.4	689.8	616.4
46	280.2	25.0	230.6	225.8	959.4	947.9
47	314.3	22.2	233.0	224.4	1091	1101
48	352.5	23.8	229.2	226.9	1001	972
49	438.8	20.5	237.8	224.6	1206	1213
50	495.4	18.9	230.6	225.2	1269	1246
51	549.1	16.2	233.3	223.7	1498	1528
52	659.5	12.3	235.4	221.9	1990	2084
53	727.4	11.9	235.0	222.4	2054	2136
54	812.3	8.5	239.8	221.0	2934	3113
55	873.1	9.2	235.0	220.2	2657	2851
56	949.5	7.9	237.1	220.6	3121	3330
57	1023	6.8	236.2	219.7	3613	3905
58	1105	5.8	237.6	219.7	4261	4606
59	1163	5.4	236.2	218.9	4550	4973
60	1232	5.2	235.2	219.0	4705	5138
61	1283	5.2	235.2	219.0	4705	5138
62	1382	3.6	238.6	219.0	6894	7528
63	1312	4.7	236.6	219.0	5236	5718
64	1307	4.3	244.8	217.2	5921	6626
65	1244	4.6	236.6	217.0	5350	6003
66	1181	5.4	237.4	217.4	4572	5102
67	1399	4.1	235.2	218.8	5967	6535
68	1402	4.7	233.5	219.6	5167	5591
69	1077	6.2	236.4	220.9	3966	4210
70	1013	7.4	233.0	221.5	3275	4450

Run	Pressure *	Δt	$\frac{dt}{dx}$	Mean Temp Interface	Observed h	h Corrected to 225 °F
	lb/in. ²	°F	°F/ft	°F	BTU/hr. ft ² °F	BTU/hr. ft ² °F
71	936.7	8.0	234.2	221.9	3045	3188
72	871.7	9.7	231.8	223.2	2485	2552
73	792.5	9.0	236.6	222.5	2734	2837
74	728.8	10.6	234.2	222.6	2298	2383
75	632.6	12.4	235.0	223.8	1971	2006
76	567.5	13.2	235.7	224.9	1857	1860
77	495.4	15.2	235.2	222.2	1609	1678
78	437.4	15.7	240.0	221.6	1590	1673
79	362.4	17.1	243.4	222.4	1480	1539

Radiation Runs - Specimens 3

80	0	220.2	2.16	177.7	1.02	
81	0	221.8	3.36	178.7	1.58	
82	0	116.0	6.48	135.0	5.81	
83	0	113.0	9.6	132.0	8.84	
84	0	115.1	8.64	133.8	7.81	
85	0	113.6	12.0	133.9	10.99	

Vacuum Runs - Specimens 3

86	8.9	38.3	232.3	247.4	630.9	480.7
87	8.9	36.3	229.9	246.2	658.8	510.6
88	24.5	31.2	229.4	241.9	764.8	627.9
89	21.6	22.2	138.2	174.9	647.5	992.0
90	147.5	27.6	317.3	302.3	1196	532
91	105.1	23.9	230.9	237.4	1005	872
92	187.2	18.8	232.8	233.4	1288	1173
93	307.4	16.1	231.4	228.8	1495	1435
94	71.2	24.9	231.4	234.8	966.7	866.2
95	140.5	20.9	233.3	231.8	1161	1077
96	222.5	15.4	234.5	230.1	1584	1498
97	332.9	11.2	237.4	227.6	2205	2143
98	412.1	11.5	233.0	227.8	2108	2045
99	526.7	8.4	237.1	225.0	2936	2936
100	622.8	10.6	238.3	225.3	2338	2331
101	709.1	9.7	241.4	224.9	2588	2592
102	788.4	6.2	236.9	221.8	3974	4109
103	789.8	7.5	234.5	220.6	3252	3405
104	788.4	5.6	235.7	221.5	4378	4540
105	788.4	5.1	237.6	222.0	4846	4996
106	788.4	5.4	237.4	221.6	4573	4738
107	788.4	5.6	235.2	221.4	4369	4535
108	794.0	4.9	237.1	220.8	5033	5259

Run	Pressure *	Δt	$\frac{dt}{dx}$	Mean Temp Interface	Observed h	h Corrected to 225 °F
	lb/in. ²	°F	°F/ft	°F	BTU/hr. ft ² °F	BTU/hr. ft ² °F
109	796.8	4.8	237.1	220.0	5138	5410
110	932.6	3.7	236.4	219.0	6646	7071
111	1051	2.5	238.1	218.0	9906	10639
112	1216	2.0	236.9	212.6	12320	13946
113	1170	3.5	191.8	192.8	5700	7649
114	1286	2.2	279.6	244.9	13220	10431
115	1211	2.2	247.2	214.4	11680	12871
116	1344	2.0	235.4	207.7	12240	14492
117	1302	1.6	237.6	207.6	15440	18296
118	1170	2.3	233.5	213.6	10560	11838
119	1033	3.5	235.7	215.8	7000	7686
120	897.3	5.1	237.6	217.2	4846	5248
121	775.6	11.6	229.4	219.2	2057	2185
122	641.2	13.9	234.7	222.0	1756	1812
123	492.7	16.5	241.0	226.8	1519	1548
124	341.3	22.9	234.7	232.8	1066	978
125	339.9	23.5	233.8	233.6	1034	962
126	270.6	28.1	234.7	235.2	868.8	775.8

Air Runs - Specimens 3

127	11.6	46.2	200.2	253.3	450.7	256.0
128	13.0	22.1	207.4	227.4	976.1	940.0
129	62.5	15.2	209.8	214.2	1435	1693
130	133.3	10.7	209.3	208.4	2034	2549
131	196.9	7.5	207.1	199.8	2872	3975
132	232.3	7.3	246.7	223.0	3515	3624
133	318.6	5.3	226.8	205.3	4451	5786
134	496.8	3.1	254.9	217.4	8553	9545
135	607.1	2.4	251.5	215.9	10900	12415
136	727.4	2.1	252.7	215.4	12510	14336
137	905.6	1.7	255.2	214.8	15620	18057
138	1053	1.4	254.4	213.5	18900	22208
139	1073	1.2	272.4	228.5	23610	24861
140	1023	1.5	229.0	202.6	15880	21311
141	1183	1.3	253.4	215.5	20280	23221
142	1290	1.1	253.4	215.0	23960	27602
143	1273	1.2	253.4	215.0	23960	27602
144	1140	1.3	249.1	214.6	19890	23053
145	1024	1.5	248.6	215.4	17230	19746
146	880.1	1.6	250.6	216.1	16290	18505
147	727.4	2.0	251.0	216.8	13050	14681

Run	Pressure *	t	$\frac{dt}{dx}$	Mean Temp Interface	Observed h	h Corrected to 225 °F
	lb/in. ²	°F	°F/ft	°F	BTU/hr, ft ² °F	BTU/hr, ft ² °F
148	571.7	2.2	251.8	216.9	11900	13367
149	520.8	2.7	250.6	217.0	9654	10832
150	376.5	3.7	248.2	217.6	6977	7765
151	290.2	4.8	255.1	219.4	5528	5998

Vacuum Runs - Specimens 3

152+	126.3	36.3	220.3	218.6	631.2	674.1
153	223.5	16.3	236.6	216.7	1509	1637
154	325.7	10.1	253.9	229.2	2614	2496
155	380.9	7.3	253.9	226.6	3617	3556
156	433.3	6.2	254.9	226.9	4276	4190
157	529.4	5.2	253.7	224.9	5074	5079
158	614.3	4.2	255.4	224.1	6325	6385
159	639.8	4.6	276.5	237.6	6252	5414
160	593.1	4.7	231.8	210.2	5130	5935
161	659.6	4.6	254.6	222.5	5757	5912
162	750.1	3.7	255.8	221.8	7191	7435
163	809.5	4.2	254.9	222.7	6313	6465
164	878.9	3.9	252.0	221.9	6721	6943
165	945.3	2.8	258.2	222.3	9592	9870
166	1041	3.4	253.9	221.2	7767	8078
167	1115	3.0	253.9	221.2	8803	9155
168	917.1	2.9	253.9	221.8	9107	9417
169	634.2	5.7	255.4	222.8	4661	4768
170	637.0	4.4	246.7	216.1	5832	6380
171	634.2	5.8	233.5	209.8	4187	4861
172	635.5	5.1	268.3	230.1	5472	4977
173	635.5	5.1	283.2	238.8	5776	4962
174	441.7	7.2	235.2	216.2	3397	3713

Air Runs - Specimens 1

175	43.4	2.0	244.8	240.8	12730	9662
176	64.6	2.2	238.1	236.9	11250	9214
177	104.9	0.9	239.0	234.8	27620	23505
178	6.0	5.8	167.0	189.7	2995	4606
179	6.0	7.2	193.9	211.6	2801	3372
180	6.0	6.6	175.2	199.1	2761	3852

Air Runs - Specimens 4 - Flat

181	6.0	18.0	208.8	219.6	1206	1305
182	6.0	19.2	206.9	221.1	1120	1186
183	243	8.4	212.2	203.7	2627	3481

Run	Pressure *	Δt	$\frac{dt}{dx}$	Mean Temp Interface	Observed h	h Corrected to 225 °F
	lb/in. ²	°F	°F/ft	°F	BTU/hr. ft ² °F	BTU/hr. ft ² °F
184	613	4.4	208.8	195.2	4936	7177
185	613	4.9	246.7	223.6	5237	5347
186	809	3.8	248.6	222.5	6805	7064
188	1045	2.3	250.3	222.4	11320	11773
189	1164	1.7	252.2	222.4	15430	16047
190	1375	0.4	252.0	221.7	65530	68806
191	1256	0.8	249.8	221.7	32480	34104
192	1037	1.8	250.6	223.1	14480	14900
193	828	2.4	250.1	220.1	10830	11642
194	605.7	2.8	254.4	224.2	9450	9563
195	457.2	3.8	254.9	224.5	6977	7033
196	189.8	11.7	234.2	222.7	2082	2155
197	113.4	16.4	233.5	225.5	1481	1469
198	1.2	60.4	178.1	227.4	307.7	296.4

Vacuum Runs - Specimens 4 - Flat

199	219.5	50.8	208.8	226.9	427.5	418.9
200	246.4	44.3	187.2	215.1	439.5	461.2
201	281.9	39.7	186.2	208.7	487.8	572.2
202	445.8	27.0	231.4	225.6	891.4	886.1
203	602.8	14.0	240.0	217.6	1783	1924
204	850.4	10.2	255.8	224.7	2609	2617
205	1061	7.3	256.3	223.3	3652	3718
206	1292	4.6	268.8	228.7	6078	5846
207	1408	4.0	269.8	229.0	7016	6735
208	1207	5.3	259.2	221.4	5087	5280
209	976	8.8	255.8	224.2	3023	3047
210	770	12.6	260.2	227.0	2148	2103
211	108	59.6	223.7	244.5	392	311

TABLE B-2 -- Data for Curves of Table B-1

Pressure *	h_T	h_v	h_a	h_a/h_T	$R \times 10^4$
lb/in^2	$\text{BTU/hr. ft}^2 \text{ } ^\circ\text{F}$	$\text{BTU/hr. ft}^2 \text{ } ^\circ\text{F}$	$\text{BTU/hr. ft}^2 \text{ } ^\circ\text{F}$	Dimensionless	Dimensionless
Specimen 4 - Non-Flat					
0	190	50	140	.737	0.594
100	400	100	300	.750	0.554
200	650	170	480	.738	0.589
300	910	260	650	.714	0.665
400	1180	380	800	.677	0.789
500	1490	520	970	.651	0.891
600	1840	690	1150	.625	0.997
700	2240	870	1370	.611	1.05
800	2700	1040	1660	.614	1.04
900	3210	1280	1930	.601	1.10
1000	3780	1520	2260	.597	1.12
1100	4430	1790	2640	.595	1.13
1200	5170	2070	3100	.599	1.11
1300	5990	2380	3610	.602	1.10
1400	6970	2700	4270	.612	1.05
Specimen 4 - Flat					
0	990	180	810	.818	0.369
100	1720	280	1440	.837	0.323
200	2500	370	2130	.852	0.289
300	3360	530	2830	.842	0.311
400	4330	730	3600	.831	0.337
500	5380	1020	4360	.810	0.389
600	6570	1370	5200	.791	0.438
700	7920	1790	6130	.773	0.485
800	9380	2280	7100	.756	0.534

* Pressure is "apparent" interface pressure

Pressure *	h_T	h_v	h_a	$h_{a/T}$	$R \times 10^4$
lb/in^2	BTU/hr. ft^2 °F	BTU/hr. ft^2 °F	BTU/hr. ft^2 °F	Dimensionless	Dimensionless
900	11020	2830	8190	.743	0.574
1000	12860	3480	9380	.729	0.617
1100	14970	4180	10790	.720	0.644
1200	17330	4970	12360	.713	0.668
Specimen 3					
0	920	780	140	.152	9.26
100	2130	910	1220	.573	1.24
200	3820	1110	2710	.709	0.681
300	5830	1380	4450	.763	0.515
400	7830	1730	6100	.779	0.471
500	9830	2220	7610	.774	0.485
600	11830	2800	9030	.763	0.515
700	13830	3530	10300	.744	0.570
800	15840	4510	11330	.715	0.661
900	17880	5720	12160	.680	0.782
1000	19910	7120	12790	.642	0.925
1100	21920	8820	13100	.597	1.12
1200	23920	10930	12990	.543	1.40
1300	25920	13560	12360	.476	1.82

TABLE B-3 -- Meyer Hardness

Ball Size mm	Load Kgm	Rockwell Hardness	Indentation Diameter mm	Dia. Indentation Dia. Ball	Meyer Hardness	
					Kgm/mm ²	lb./in. ²
3.175	100	89.8E	1.14	.359	97.9	139,000
	100	89.9E	1.13	.356	99.6	141,400
	100	89.8E	1.15	.362	96.2	136,500
Average						138,900
3.175	150	67.7K	1.37	.431	101.6	144,200
	150	68.4K	1.38	.435	100.2	142,200
	150	69.0K	1.38	.435	100.2	142,200
Average						142,800
1,5875	45	45-T-18	0.75	.472	101.8	144,500
	45	45-T-28	0.75	.472	101.8	144,500
	45	45-T-31	0.75	.472	101.8	144,500
Average						144,500
Overall Average						142,000

TABLE B-4 -- Surface Roughness

Specimen	Before Loading (A)		Before Loading (B)		After Loading (C)		Mean Values	
	RMS	Arith Avg	RMS	Arith Avg	RMS	Arith Avg	RMS	Arith Avg
1 Upper	20.3	16.7	15.4	12.0	7.2	5.5		
	9.5	7.9	10.2	8.1	11.3	8.5		
	9.7	7.4	13.1	9.3	9.1	7.4		
	8.7	6.9	13.0	10.3	10.6	8.3		
	9.9	8.1	8.7	7.0				
Average	11.4	9.4	12.0	9.3	9.6	7.4		
Max Peak-To-Valley		120		84		130		
1 Lower	6.6	5.7	11.7	7.9	6.8	5.5		
	8.5	7.1	12.6	8.4	8.1	6.2		
	11.0	9.4	8.7	7.2	7.9	5.3		
	8.0	7.1	8.6	6.8	9.0	7.3		
			6.6	5.5	5.5	4.6		
Average	8.5	7.3	9.6	7.2	7.5	5.8	9.7	7.4
Max Peak-To-Valley		110		90		110		110
2	Not Used				Average		31.6	
3 Upper	143	120	128	101	132	103		
	168	144	121	94	135	103		
	163	137	117	96	116	90		
	129	111	131	105	135	108		
			134	113	126	101		
Average	150	128	126	102	129	101		
Max Peak-To-Valley		700		900		610		

Specimen	Before Loading (A)		Before Loading (B)		After Loading (C)		Mean Values	
	RMS	Arith Avg	RMS	Arith Avg	RMS	Arith Avg	RMS	Arith Avg
3 Lower	170	134	104	82	143	116		
	175	141	127	110	115	90		
	143	116	148	119	151	121		
	120	103	134	118	147	124		
	134	109			141	115		
Average	148	121	128	107	139	113	136	111
Max Peak-To-Valley		900		900		600		727
4 Upper	72.4	67.0			68.7	56.7		
Non-Flat	63.1	56.7			108.3	88.0		
	70.4	62.2			85.0	61.0		
	68.3	60.5			95.1	75.3		
					107.0	78.7		
Average	66.0	61.6			92.8	71.9		
Max Peak-To-Valley		440				500		
4 Lower	66.7	59.6			45.6	34.7		
Non-Flat	44.1	39.4			67.9	52.0		
	55.7	47.6			29.4	22.7		
	53.8	45.2			77.8	60.7		
					64.6	46.7		
Average	55.1	47.9			57.1	43.4	67.8	56.2
Max Peak-To-Valley		380				410		432
4 Upper			10.1	8.6	10.3	8.7		
Flat			9.9	8.0	8.5	7.3		
			11.4	8.9	9.8	8.4		
			7.9	6.4	8.0	6.6		
					5.9	4.7		
Average			9.8	8.0	8.5	7.1		
Max Peak-To-Valley					83	61		

Specimen	Before Loading (A)		Before Loading (B)		After Loading (C)		Mean Values	
	RMS	Arith Avg	RMS	Arith Avg	RMS	Arith Avg	RMS	Arith Avg
4 Lower			10.8	9.0	4.9	3.8		
Flat			11.2	8.4	10.1	8.6		
			9.1	7.6	7.0	5.6		
			11.2	8.7	6.6	5.0	9.0	7.3
Average			10.6	8.4	7.2	5.8		80
Max Peak-To-Valley				100		76		

A Readings taken at China Lake.

B and C Readings taken at U. S. Naval Postgraduate School.

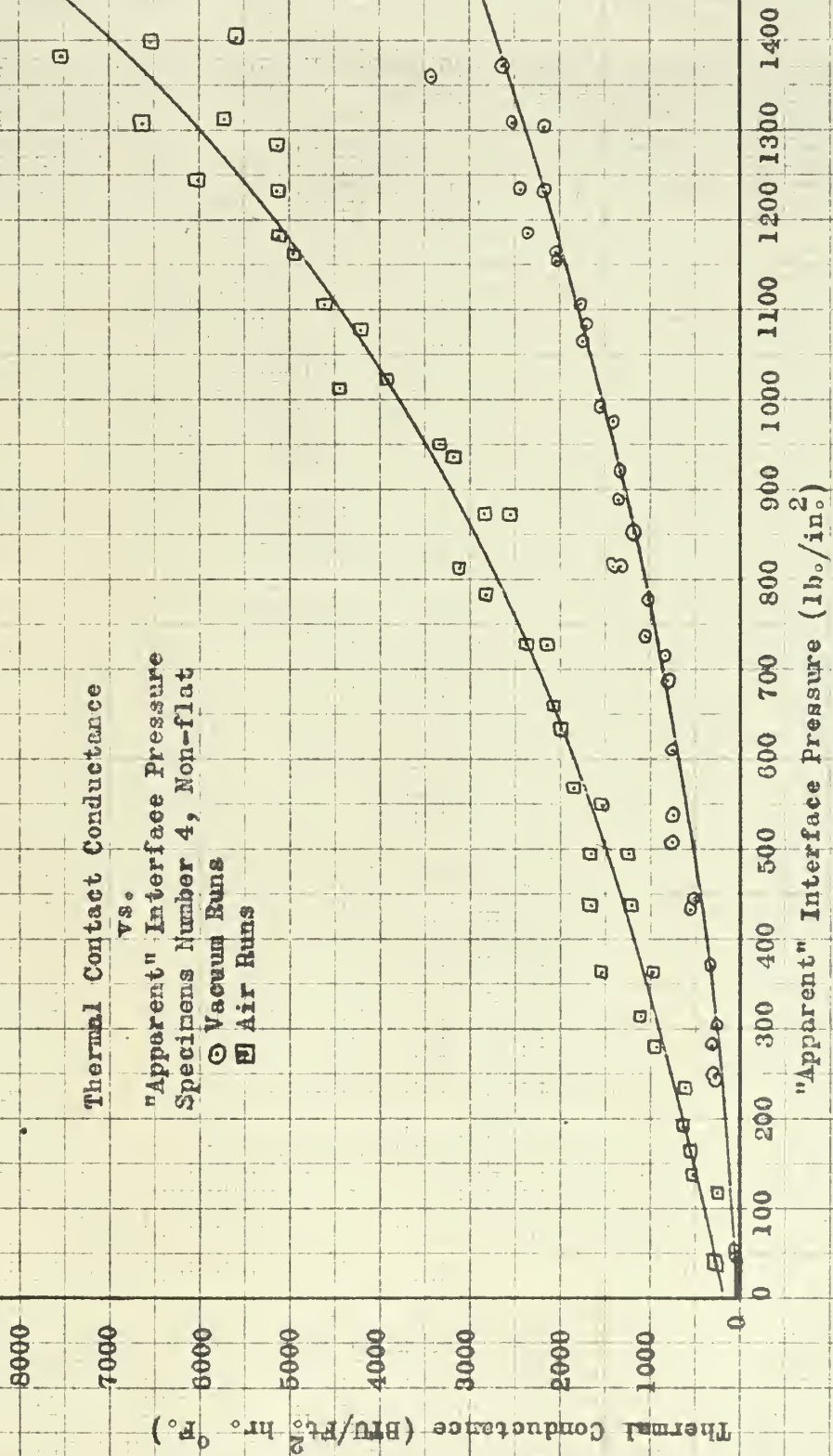
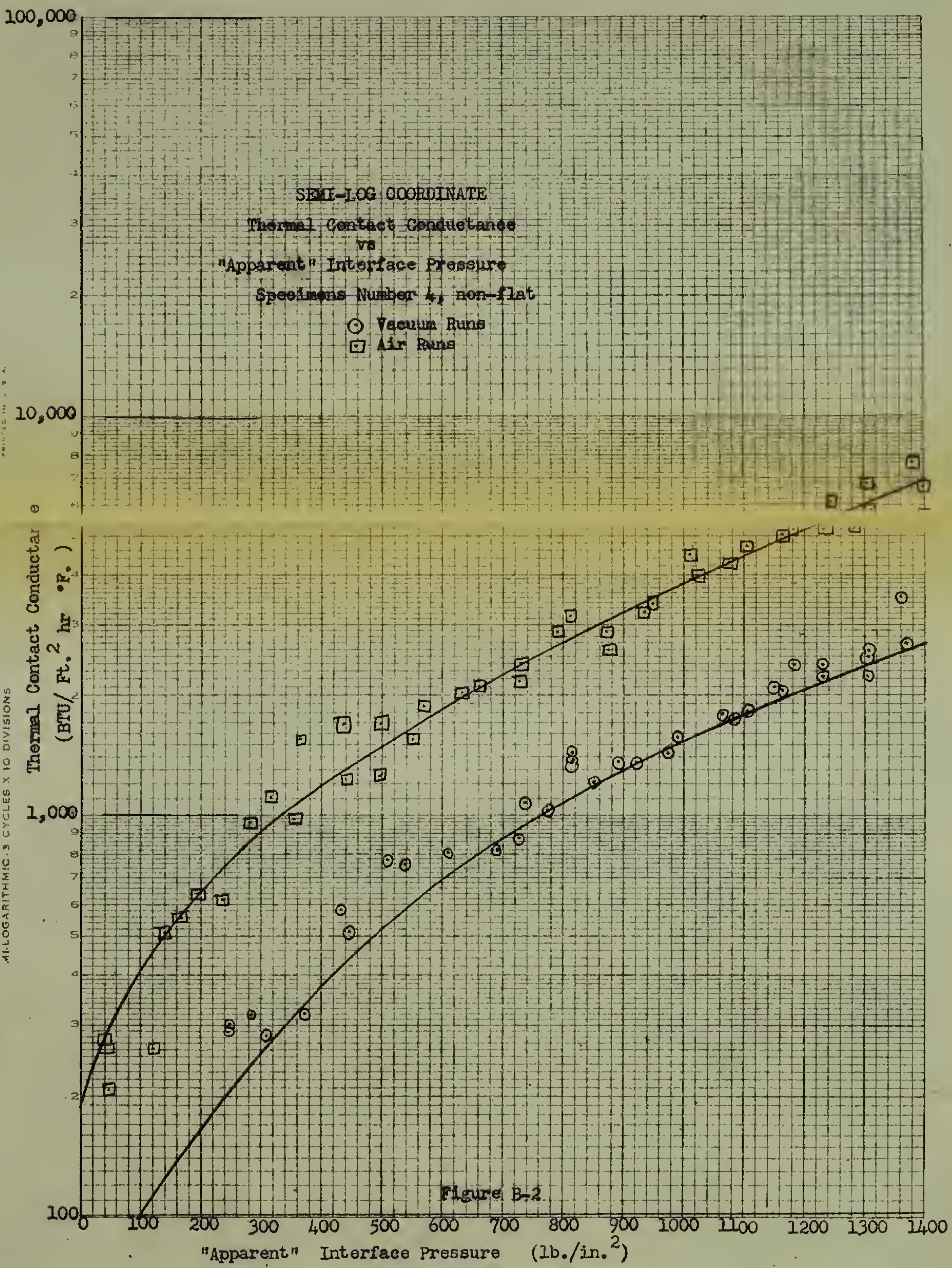


Figure B-1



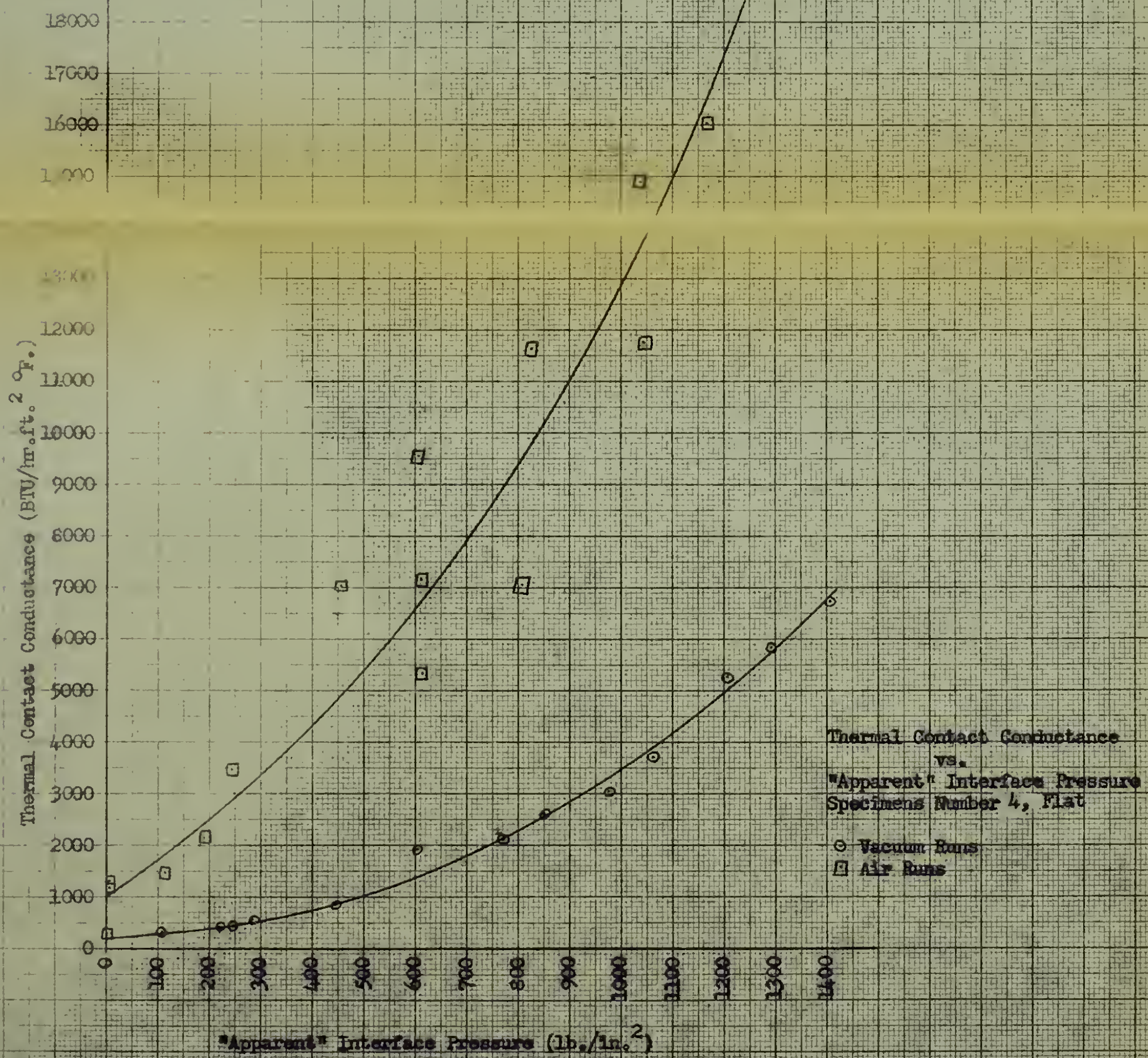
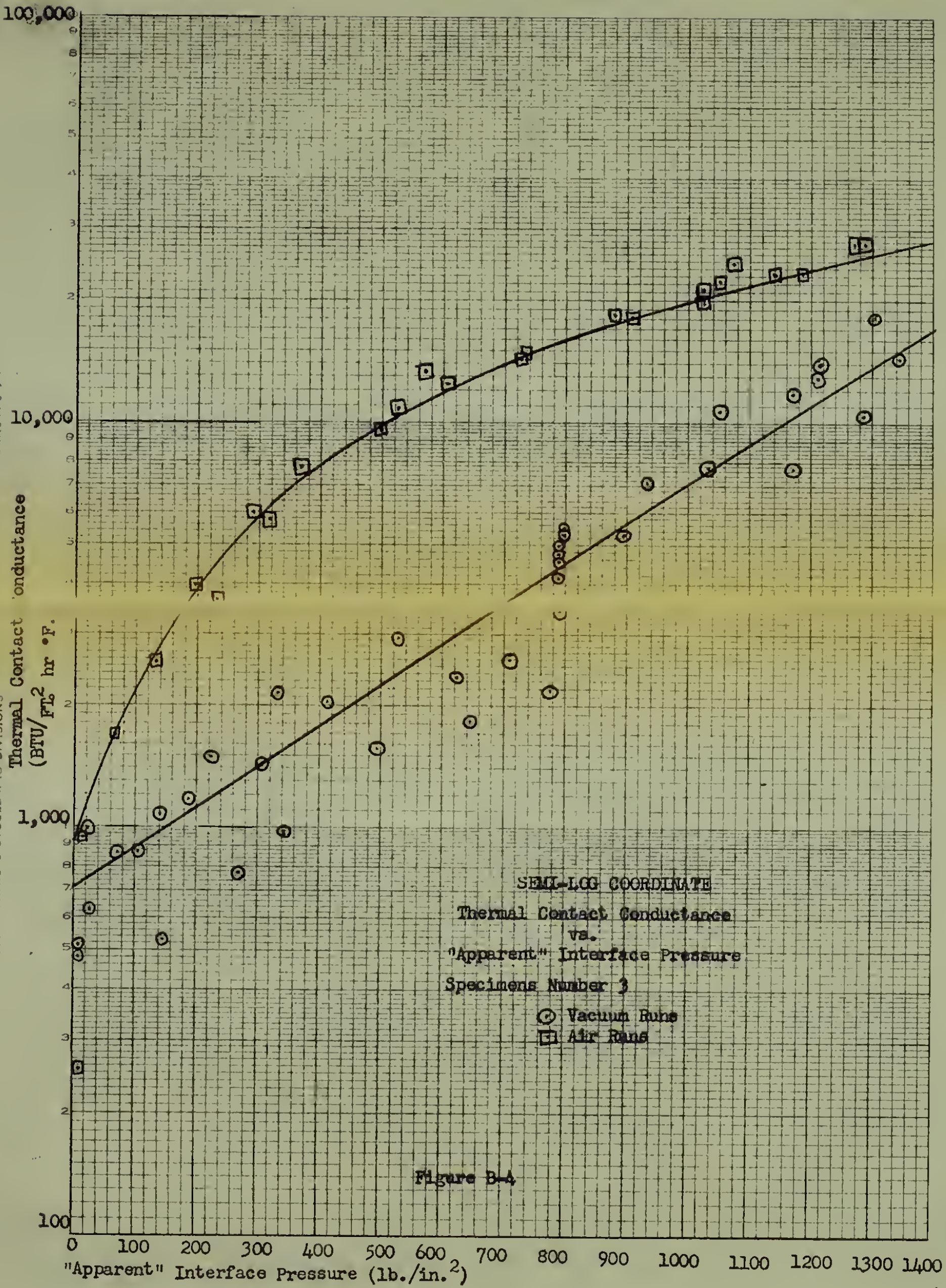


Figure B-3



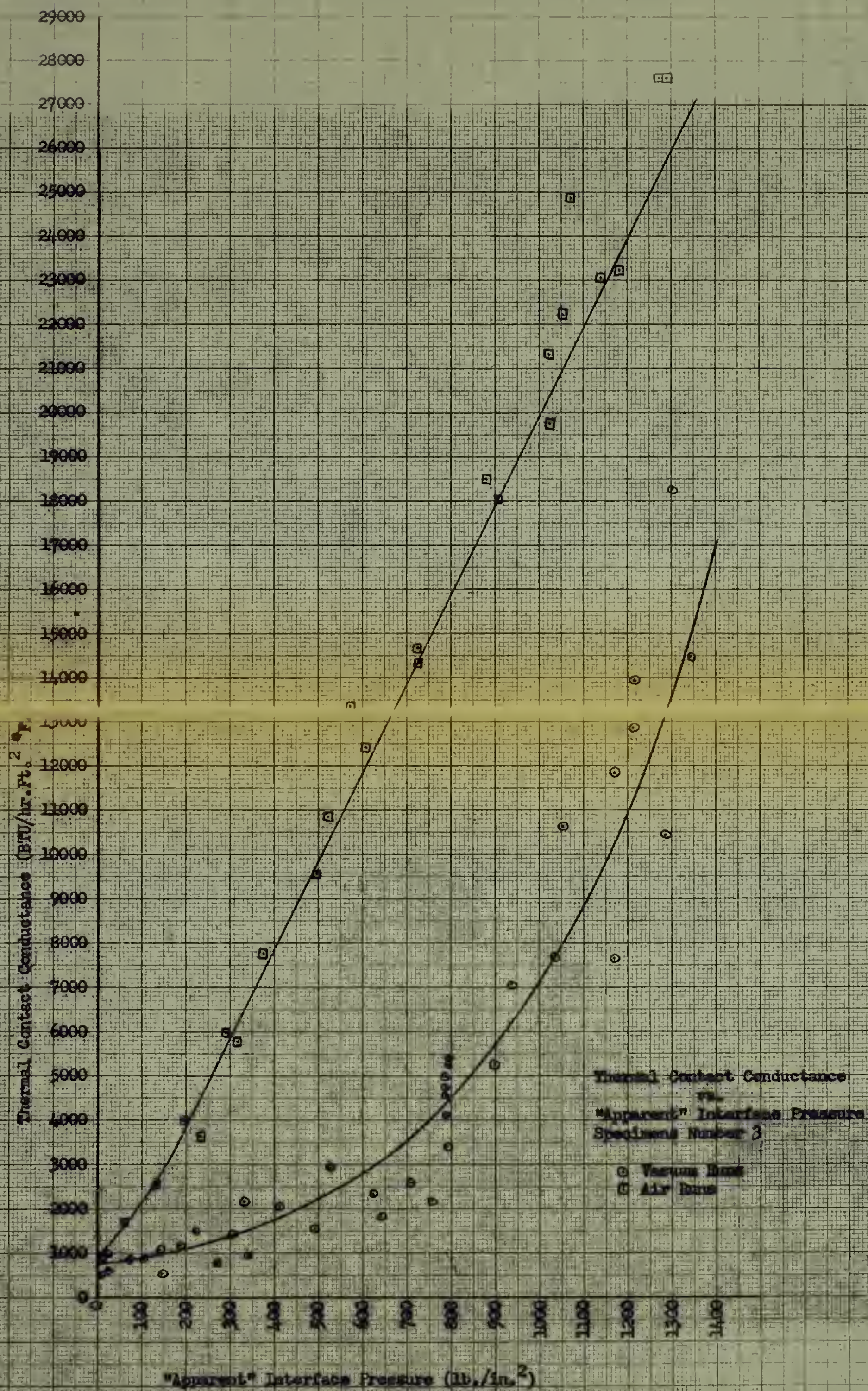
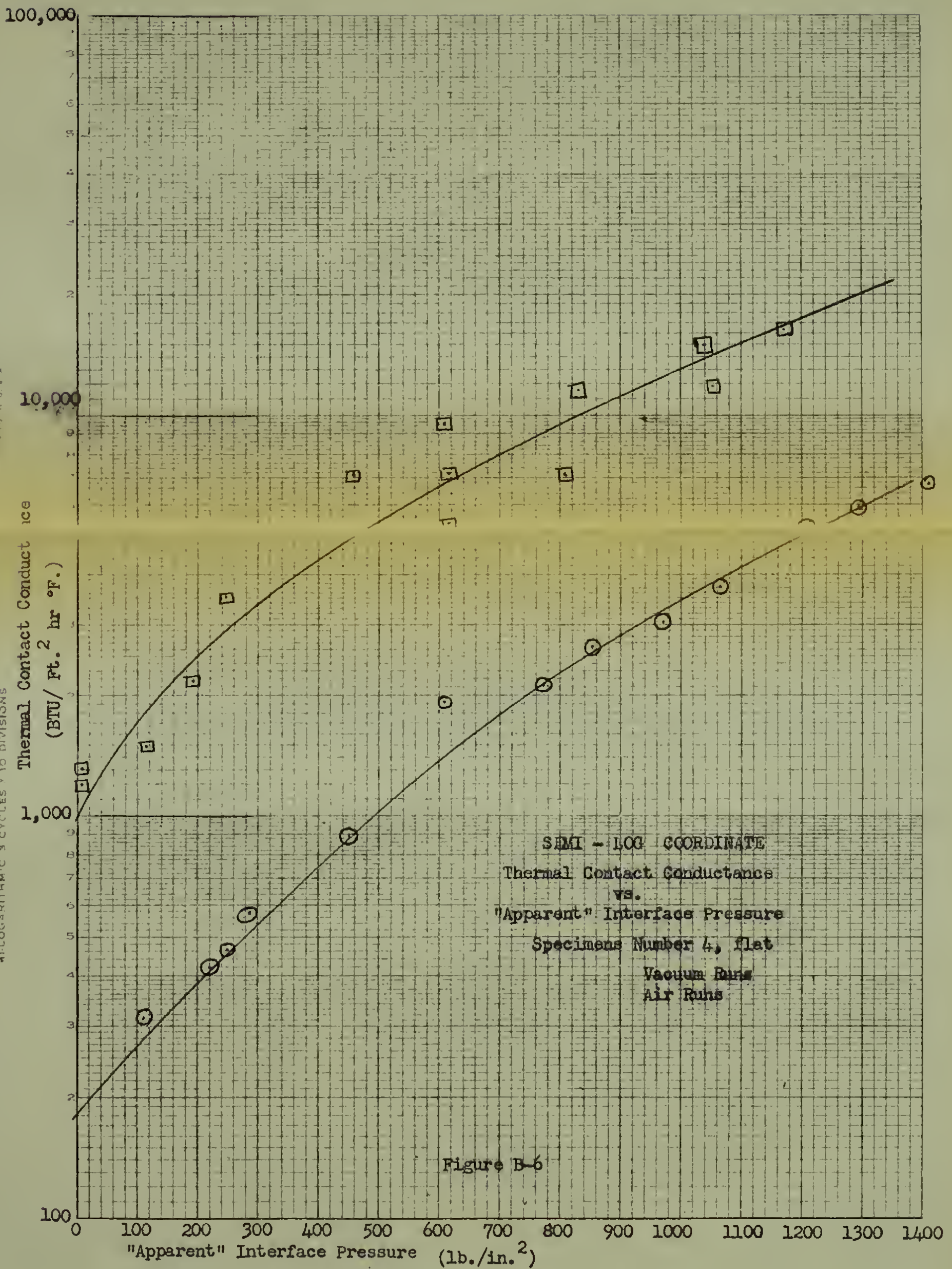


Figure B-5

98

NO. 340-L310 DIETZGEN GRAPH PAPER
41-LOGARITHMIC 3 CYCLES X 10 DIVISIONS

W. E. DIETZGEN CO
NEW YORK, N. Y. U. S. A.



Mean Interface Temperature ($^{\circ}\text{F}$)

230
220
210
200

Air Run

16000 17000 18000 19000 20000 21000 22000 23000

Thermal Contact Conductance ($\text{BTU/hr. ft}^2 \text{ } ^{\circ}\text{F}$)

Figure B-7

Mean Interface Temperature ($^{\circ}\text{F}$)

240
230
220
210
200

Thermal Contact
Conductance

vs.

Mean Interface
Temperature

Vacuum Run

4000 5000 6000

Thermal Contact Conductance
($\text{BTU/hr. ft}^2 \text{ } ^{\circ}\text{F}$)

Figure B-8

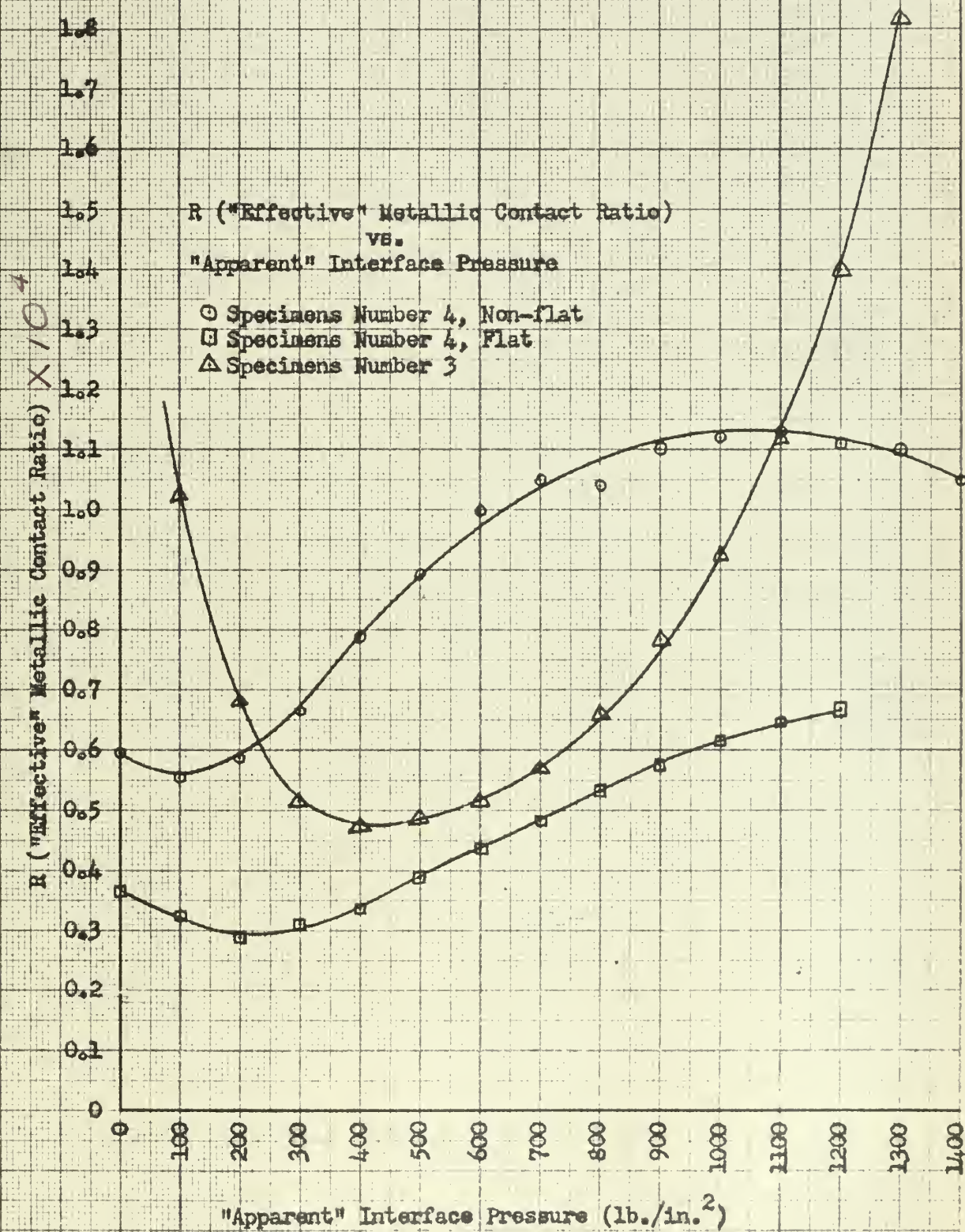


Figure B-9

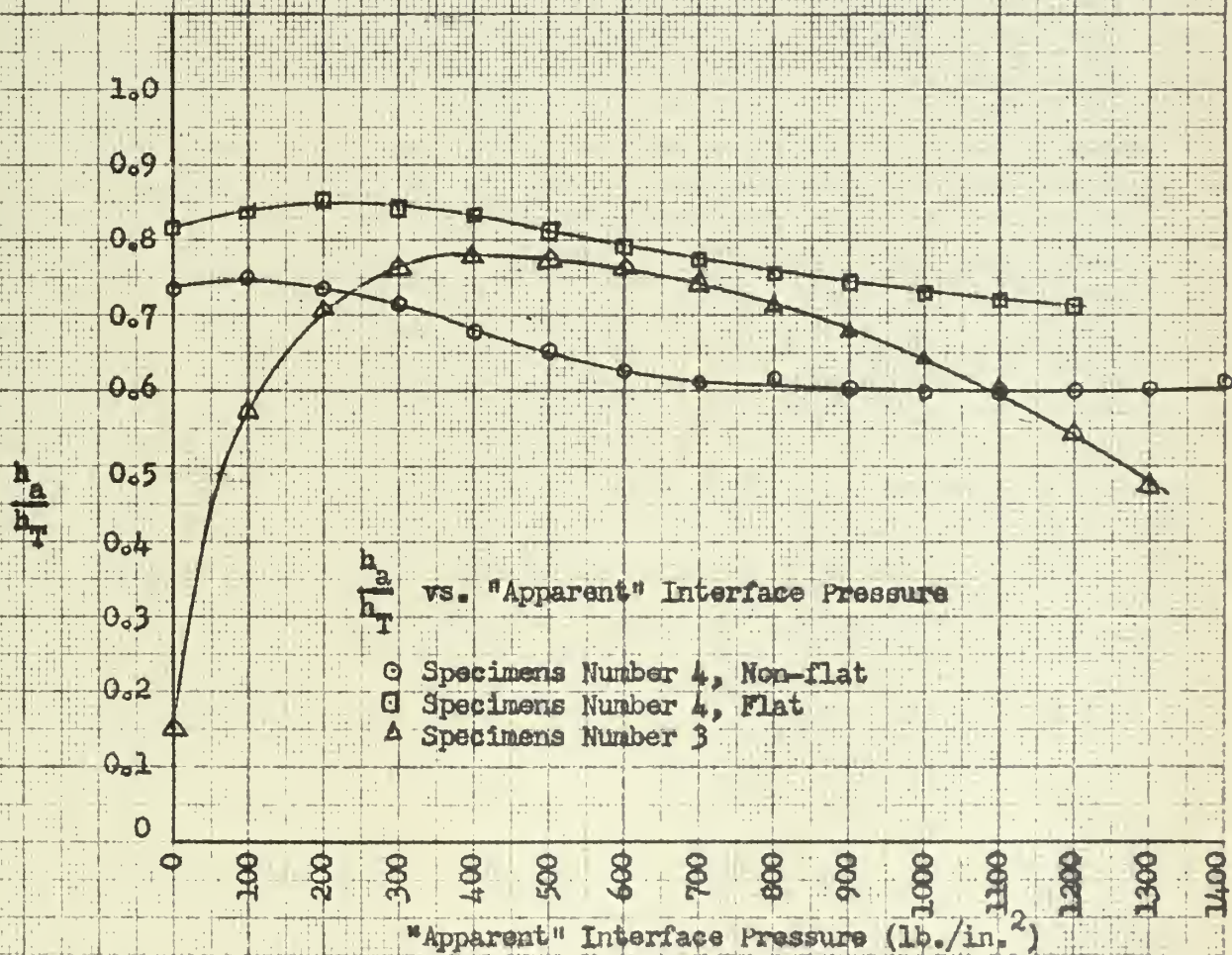


Figure B-10

APPENDIX C

DEVELOPMENT OF SHAPE FACTOR, R, "EFFECTIVE" METALLIC CONTACT RATIO

At high pressures, i.e., $\lambda \ll s$, the true value of the mean free path of the gas molecules is used. From the kinetic theory of gases (22) the value of thermal conductivity of the included gas is:

$$k_a = \frac{Cu\lambda}{3}$$

$$\lambda = \frac{6.43 \times 10^{-3}}{P} \text{ cm} \quad (\text{from Appendix D})$$

at atmospheric pressure

$$\lambda = \frac{6.43 \times 10^{-3}}{760} = 8.46 \times 10^{-6} \text{ cm}$$

Since the minimum s is of the order of 10 microinches ($2.54 \times 10^{-5} \text{ cm}$)

$\lambda \ll s$ and the condition is fulfilled.

For the air runs

$$k_a = \frac{2.11 \times 10^{-7} P \text{ cal.} \times 5.27 \times 10^4 \text{ cm} \times 6.43 \times 10^{-3} \text{ cm}}{\text{cm}^3 \text{ } ^\circ\text{C} \quad \text{sec} \quad P}$$

$$k_a = 7.15 \times 10^{-5} \text{ cal/sec cm } ^\circ\text{C}$$

Using the resistance model described in the Introduction and neglecting the heat transferred by radiation,

$$h_T = h_a + h_m$$

Since there is no heat transferred across the interface by conduction through the air during a vacuum run as shown in Appendix D, it is assumed that the values of conductance obtained by the vacuum runs are valid for the conductances due to the metallic contact during the air runs. Hence

$$h_T = h_a + h_m = h_a + h_v$$

By definition

$$q + hA \Delta t$$

Hence

$$q_T = h_T A \Delta t$$

$$q_v = h_v A \Delta t$$

$$\text{and } q_a = h_a A \Delta t$$

$$\text{Thus } q_T = q_a + q_m = (h_a + h_v) A \Delta t$$

But also using Fourier's Law of Heat Transfer

$$q = -kA \frac{dt}{dx}$$

$$q_a = -k_a A_a \frac{dt}{dx}$$

$$\text{and } q_m = -k_m A_m \frac{dt}{dx}$$

$$q_T = (h_a + h_v) A \Delta t = -(k_a A_a \frac{dt}{dx} + k_m A_m \frac{dt}{dx})$$

Since the gap distance is small $\frac{\Delta t}{s}$ can be used as a good approximation for $\frac{dt}{dx}$. It should be realized that if an equal Δt is used, the distance s will, in general, not be the same for the air and metal paths of thermal current flow.

$$h_a A = - \frac{k_a A_a}{s_a}$$

$$h_v A = - \frac{k_m A_m}{s_m}$$

$$\frac{A_m}{A_a} = \frac{h_v A_s k_a}{h_a A_s k_m} = \frac{h_v k_a s_m}{h_a k_m s_a}$$

From this a shape factor, the "effective" metallic contact ratio is defined as:

$$R \equiv \frac{A_m s_a}{A_a s_m} = \frac{h_v k_a}{h_a k_m}$$

As an example, using Helium as the included medium:

$$k_a = 0.099 \text{ BTU/hr. ft.}^2 \text{ } ^\circ\text{F/ft.}$$

$$\frac{k_a}{k_m} = \frac{0.099}{104.0} = 9.52 \times 10^{-4}$$

$$\frac{h_a}{h_v} = \frac{k_a}{k_m} \times \frac{1}{R}$$

$$h_T = h_a + h_v = h_a \left(1 + \frac{k_m R}{k_a}\right)$$

$$\frac{h_a}{h_T} = \frac{1}{1 + \frac{k_m R}{k_a}}$$

Using a typical value for specimen 4, non-flat at 900 pounds per square inch "apparent" interface pressure $\frac{h_a}{h_T} = 0.601$ for air and $R = 1.10 \times 10^{-4}$.

Using the conductivity of Helium and the equation above:

$$\frac{h_a}{h_T} = \frac{1}{1 + \frac{1.10 \times 10^{-4}}{9.52 \times 10^{-4}}} = \frac{1}{1 + .116} = .90$$

or 90% of the heat would be transferred by conduction through the Helium whereas only 60% of the heat was transferred through the air. Since the quantity of heat transferred through the metal remains the same the total heat transferred is increased proportionately.

APPENDIX D

HEAT FLOW ACROSS A GAS-FILLED GAP AT LOW PRESSURES

The following is a summary of a theoretical determination of the heat flow across a small gas-filled gap at low pressure. This determination was suggested by E. C. Crittenden, Jr., Professor of Physics, U. S. Naval Postgraduate School, Monterey, California.

Symbols:

k = Thermal conductivity of air (cal./cm.² °C./cm.)

c = Molecular heat capacity of air (cal./ °C. molecule)

u = Mean molecular velocity of air (cm./sec.)

λ = Mean free path of air molecules (cm.)

α = Constant factor, defined in the development of the problem

β = Accommodation coefficient

A = Area, see Figure D-1

Θ = Angle, see Figure D-1

$d\omega$ = Differential solid angle = $\frac{dA}{r^2}$

N' = Number of particles per unit volume per unit solid angle per unit area

N = Number of particles per unit volume

s = Gap distance (cm.), see Figure D-1 and Figure D-2

dn = Number of particles per unit time per unit solid angle impinging on a unit area

n = flux = Number of particles per unit time impinging on a unit area

Δq = Differential energy transferred per particle per unit area

ΔT = Temperature difference between the surfaces

q = Energy transferred to the surface per unit area (cal./cm.²)

Q = Energy transferred to the surface (cal.)

C = Nc = Heat capacity or specific heat per unit volume (cal/cm.³ °C.)

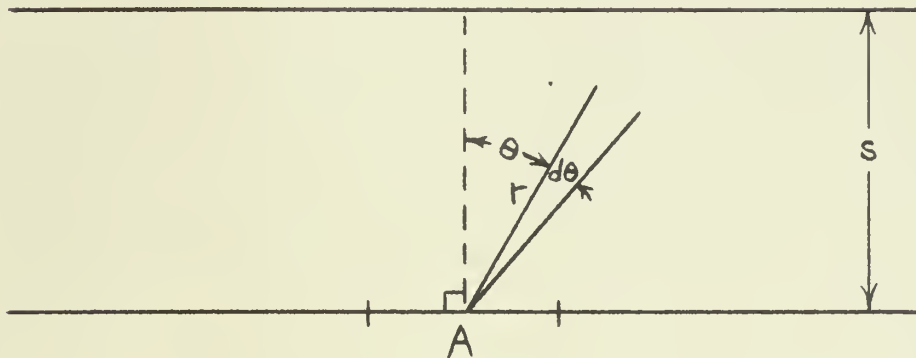


Figure D-1

Provided that λ is very large relative to s , then only wall collisions are of importance. The number of particles per unit time per unit solid angle impinging on area A equals $N' Au \cos \theta d\omega$

$$dn = N' u \cos \theta d\omega$$

$$d\omega = \frac{2\pi r d\theta \cdot r \sin \theta}{r^2} = 2\pi \sin \theta d\theta$$

$$dn = 2\pi N' u \sin \theta \cos \theta d\theta$$

$$n = 2\pi \int_0^{\pi/2} N' u \sin \theta \cos \theta d\theta = 2\pi \int_0^1 N' u \sin \theta (d \sin \theta)$$

$$n = 2\pi N' u \left[\frac{\sin^2 \theta}{2} \right]_0^{\pi/2} = \pi N' u$$

$$\text{But, } N' = \frac{N}{4\pi}$$

$$\text{so } n = \frac{N \pi u}{4\pi} = \frac{Nu}{4}$$

Now if each particle on the average carries a net energy excess, then Δq per particle is equal to $c \Delta T$.

Or if the accommodation coefficient, β , is taken into account:

$$\Delta q = \beta^2 c \Delta T$$

β^2 is necessary because two wall-to-gas interfaces are involved.

Hence for a flux n , the heat transferred to a unit area would be:

$$\frac{dq}{dt} = n \Delta q = n \beta^2 c \Delta T = \frac{Nu \beta^2 c \Delta T}{4} \times 2 \text{ (to include the upward flux)}$$

$$\text{or } \frac{dq}{dt} = \frac{\beta^2 u C \Delta T}{2}$$

The heat transferred to the area A would be

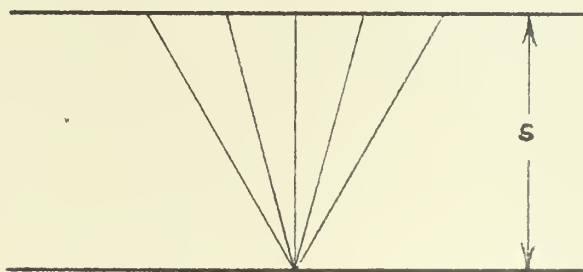
$$\frac{dQ}{dt} = \frac{\beta^2 u C A \Delta T}{2}$$

It is noted that the heat transfer is independent of the gap distance.

It should be further noted that C varies linearly with pressure.

An alternate approach to the problem is as follows:

For low pressures, the "mean free path" would be determined by the gap thickness, s . It would be a constant factor, greater than one, multiplied by the gap thickness, due to geometry, i.e., it would be averaged over all directions, as shown in Figure D-2, but limited in the parallel direction by gas-gas collision.



Note: True only if gas-gas collision free path is large compared to s .

Figure D-2

As a first approximation, assume that $\lambda = s \propto$

Now the heat transfer is

$$\frac{dQ}{dt} = kA \frac{dT}{dx} = kA \frac{\Delta T}{s} \text{ or if the accommodation coefficient is considered}$$

$$\frac{dQ}{dt} = kA \frac{\Delta T \beta^2}{s}$$

as, at the distances involved $\frac{\Delta T}{s}$ closely approximates $\frac{dT}{dx}$,

but in general from the kinetic theory of gases one finds (22) that:

$$k = \frac{Cu\lambda}{3} = \frac{Cus\alpha}{3}$$

$$\text{then } \frac{dQ}{dt} = \frac{Cus\alpha}{3} \frac{A\Delta T \beta^2}{s} = \frac{CuA\Delta T\alpha\beta^2}{3}$$

Hence $\frac{dQ}{dt}$ is independent of gap thickness.

It is interesting to compare the results of both of these lines of reasoning.

Equating the two expressions for $\frac{dQ}{dt}$

$$\frac{dQ}{dt} = \frac{\beta^2 u C A \Delta T}{2} = \frac{C \alpha u A \Delta T \beta^2}{3}$$

$$\text{and } \frac{\alpha}{3} = \frac{1}{2}$$

$$\text{or } \alpha = \frac{3}{2}$$

It is found that Sears (30) by using a different approach has evaluated a factor which is equivalent to α and has obtained a value of $\frac{3}{2}$ which agrees with this development.

Thus the two models agree.

To obtain the maximum amount of heat transferred through the air during vacuum runs:

$$\frac{dQ}{dt} = \frac{\beta^2 u C A \Delta T}{2}$$

$$\text{For air } \rho = \frac{0.001293 \text{ H}}{(1.0 + 0.00367T) 76} \quad (14)$$

where H = pressure in cm. of Hg

and T = temperature in degrees Centigrade

$$\rho = 0.001226 \text{ gm/cm}^3 \text{ at } 15^\circ\text{C. and 76 cm of Hg}$$

At 225°F. (107.2°C.)

$$\rho = \frac{0.001226 H}{(1 + 0.3934) 76} = 1.22 \times 10^{-5} H$$

$$\text{or } \rho = 1.22 \times 10^{-6} P \text{ gm/cm}^3$$

where P = pressure in mm. of Hg

$$\lambda \propto \frac{1}{\rho}$$

$$\lambda = 6.4 \times 10^{-6} \text{ cm at } 15^\circ\text{C. and 76 cm Hg pressure (22)}$$

At 225°F.

$$\lambda = \frac{6.4 \times 10^{-6} \times 0.001226}{1.22 \times 10^{-6} P} = 6.43 \times 10^{-3} / P \text{ cm}$$

For vacuum runs, i.e., $P < 1 \times 10^{-3}$ mm Hg pressure

$$\lambda = \frac{6.43 \times 10^{-3}}{1 \times 10^{-3}} = 6.43 \text{ cm}$$

Actually the vacuum observed was always closed to 1×10^{-5} mm of Hg.

Since the maximum s is of the order of 200 microinches (5.08×10^{-4} cm)

$\lambda \gg s$ and the condition placed on the development above is fulfilled.

$$u = 4.63 \times 10^4 \text{ cm/sec at } 20^\circ\text{C. and 76 cm of Hg pressure (14)}$$

$$u \propto (T)^{\frac{1}{2}}$$

At 225°F.

$$u = 4.63 \times 10^4 \times \left(\frac{380.2}{293}\right)^{\frac{1}{2}} = 5.27 \times 10^4 \text{ cm/sec}$$

$$C = \rho c_v$$

$$c_v = 0.173 \text{ BTU/lb } ^\circ\text{F.} = 0.173 \text{ cal./gm}^\circ\text{C. (18)}$$

at 225°F.

$$C = 1.22 \times 10^{-6} P \times 0.173 = 2.11 \times 10^{-7} P \text{ cal./cm}^3 \text{ } ^\circ\text{C.}$$

Assume $\beta = 1$, this being the largest factor possible and giving the maximum possible heat transferred due to this effect.

$$\frac{dQ}{dt} = \frac{1 \times 5.27 \times 10^4 \text{ cm} \times 2.11 \times 10^{-7} \times 1 \times 10^{-3} \text{ cal.} \times 7,069 \text{ in.}^2 \times (2.54)^2 \text{ cm}^2 \times 200^\circ\text{C.}}{\text{sec} \quad \text{cm}^3 \quad ^\circ\text{C.} \quad \text{in.}^2}$$

$$\frac{dQ}{dt} = 0.102 \text{ cal./sec} = 1.45 \text{ BTU/hr.}$$

This value is negligible compared with the smallest $\frac{dQ}{dt}$ obtained for a vacuum run which was:

$$q = k_m \frac{dt}{dx} = \frac{104.02 \text{ BTU} \times 7,069 \text{ in.}^2 \text{ ft}^2 \times 138.2 \text{ }^\circ\text{F.}}{\text{hr ft } ^\circ\text{F.} \quad 144 \text{ in}^2 \quad \text{ft}}$$

$$q = 705 \text{ BTU/hr}$$

It is thus demonstrated that the amount of heat transferred by conduction through the air is negligible during a vacuum run.

BIBLIOGRAPHY

1. Aluminum Company of America, Alcoa Research Laboratories, Letter dated March 7, 1957.
2. M. E. Barzelay, K. E. Tong, G. F. Holloway, Thermal Conductance of Contacts in Aircraft Joints, NACA Technical Note 3167.
3. M. E. Barzelay, K. E. Tong, G. F. Holloway, Effect of Pressure on Thermal Conductance of Contact Joints, NACA Technical Note 3295, May 1955.
4. J. R. Benford, Discussion of Reference 31, ME 76, 109, January 1954.
5. F. Boeschoten, On the Possibility to Improve the Heat Transfer of Uranium and Aluminum Surfaces in Contact, Reactor Technology and Chemical Processing, Proceedings of the International Conference on the Peaceful Uses of Atomic Energy, United Nations, 1956, Geneva Paper, P/947.
6. F. P. Bowden and D. Tabor, The Area of Contact Between Stationary and Between Moving Surfaces, Proceedings of the Royal Society of London, England, Series A, vol. 169, Dec. 1938-Mar. 1939, pp. 391-413.
7. P. W. Bridgemen, The Effect of Pressure on the Thermal Conductivity of Metals, Proceedings American Academy of Arts and Sciences 57, 108 (1921-22)
8. A. W. Brunot and F. F. Buckland, Thermal Contact Resistance of Laminated and Machined Joints, ASME Transactions 1949, vol. 71, p. 253.
9. A. W. Brunot and F. F. Buckland, Authors Closure to References 20 and 32, ASME Transactions 1949, vol. 71, p. 257.
10. T. N. Cetinkale and Dr. M. Fishenden, Thermal Conductance of Metal Surfaces in Contact, The Institution of Mechanical Engineers and ASME, Proceedings of the General Discussion on Heat Transfer, 1951, 11-13 Sept. 1951.
11. D. H. Gurinsky, W. T. Warner, J. E. Atherton, C. Binge, H. C. Cook, L. McLean, R. J. Teitel and B. Turovlin, The Fabrication of Fuel Elements for the BNL Reactor, Reactor Technology and Chemical Processing, Proceedings of the International Conference on the Peaceful Uses of Atomic Energy, United Nations, 1956, p. 221, Geneva Paper P/828.
12. J. F. Hagen and Earl E. Lindberg, Design Considerations Applying to Specification of Surface Finish for Machined Parts, GM Engineering Journal V.1, No. 7, July, Aug. 1954.

13. Charles R. Hine, Machine Tools for Engineers, McGraw-Hill Book Co., 1950.
14. C. D. Hodgman, Handbook of Chemistry and Physics, 32nd Edition, Chemical Rubber Co.
15. R. Holm, Electric Contacts, 1946, Hugo Gerbers Forlag, Stockholm.
16. R. B. Jacobs and C. Starr, Thermal Conductance of Metallic Contacts, The Review of Scientific Instruments, vol. 10, 1939, pp. 140-141.
17. Swami Jnanananda, High Vacuum, Principles, Production, and Measurement, D. Van Nostrand Company, Inc.
18. J. H. Keenan, J. Kaye, Gas Tables, John Wiley and Sons, Inc., 1945.
19. J. D. Keller, Heat Conduction in Strip Coil Annealing, Association of Iron and Steel Engineers Yearbook, 1948.
20. J. D. Keller, Discussion of reference 8, ASME Transactions 1949, vol. 71, p. 257.
21. J. D. Keller, Discussion of reference 35, ASME Transactions 1949, vol. 71, p. 266.
22. E. H. Kennard, Kinetic Theory of Gases, McGraw-Hill Book Co., 1938.
23. S. J. Kline and F. A. McClintock, Describing Uncertainties in Single-Sample Experiments, ME 75, 3 (1953).
24. W. B. Kouwenhoven and J. H. Potter, Thermal Resistance of Metal Contacts, 1948, Welding Journal, vol. 27, p. 515.
25. E. G. Loewen, Discussion of reference 31, ME, 76, 109, Jan 1954.
26. Vincent E. Lysaght, Indentation Hardness Testing, Reinhold Publishing Corp., 1949.
27. W. H. McAdams, Heat Transmission, McGraw-Hill Book Co., Inc., 1954.
28. Walter Mikelson, Surface Finish Standards, Machine Tool Blue Book, Oct. 1942, p. 85ff.
29. C. C. Perry, H. R. Lissner, The Strain Gage Primer, McGraw-Hill Book Co., Inc., 1955.
30. F. W. Sears, An introduction to Thermodynamics, Kinetic Theory of Gases, and Statistical Mechanics, Addison-Wesley Co., 1953, p. 264.
31. R. E. Sugg, An Interferometer for Examining Polished Surfaces, ME 75, 629 (1953).

32. Helmut Thielsch, Visual and Optical Evaluation of Metal Surfaces, Metal Finishing, May 1951, p. 54.
33. Myron Tribus, Discussion of reference 8, ASME Transactions 1949, vol. 71, p. 257.
34. U. S. Navy, Bureau of Ordnance, Optics Filming, OP 1512, Dec. 1945.
35. N. D. Weills and E. A. Ryder, Thermal Resistance Measurements of Joints Formed Between Stationary Metal Surfaces, ASME Transactions, 1949, vol. 71, p. 259.

OC 17 57
NO 20 57
DE 23 57
AS 10 63

4 7 6 9
4 7 6 9
4 7 6 9
1 2 6 8 8

Thesis
R254

Reams

35729

Investigation of heat
transfer modes across a
flat metallic interface.

OC 17 57
NO 20 57
DE 23 57
AS 10 63

4 7 6 9
4 7 6 9
4 7 6 9
1 2 6 8 8

Thesis
R254

Reams

35729

Investigation of heat transfer
modes across a flat metallic
interface.

thesR254

Investigation of heat transfer modes acr



3 2768 002 04996 7

DUDLEY KNOX LIBRARY